



## Long-term observational constraints of organic aerosol dependence on inorganic species in the southeast US

Yiqi Zheng<sup>1,2,\*</sup>, Joel A. Thornton<sup>3</sup>, Nga Lee Ng<sup>4,5,6</sup>, Hansen Cao<sup>7</sup>, Daven K. Henze<sup>7</sup>, Erin E. McDuffie<sup>8,9</sup>, Weiwei Hu<sup>10,11</sup>, Jose L. Jimenez<sup>11</sup>, Eloise A. Marais<sup>12</sup>, Eric Edgerton<sup>13</sup>, Jingqiu Mao<sup>1,2,\*</sup>

<sup>1</sup>Geophysical Institute, University of Alaska Fairbanks, Fairbanks, AK, USA

<sup>2</sup>Department of Chemistry and Biochemistry, University of Alaska Fairbanks, Fairbanks, AK, USA

<sup>3</sup>Department of Atmospheric Sciences, University of Washington, Seattle, WA, USA

<sup>4</sup>School of Chemical and Biomolecular Engineering, Georgia Institute of Technology, Atlanta, GA, USA

<sup>5</sup>School of Earth and Atmospheric Sciences, Georgia Institute of Technology, Atlanta, GA, USA

<sup>6</sup>School of Civil and Environmental Engineering, Georgia Institute of Technology, Atlanta, GA, USA

<sup>7</sup>Department of Mechanical Engineering, University of Colorado Boulder, Boulder, CO, USA

<sup>8</sup>Department of Physics and Atmospheric Science, Dalhousie University, Halifax, Nova Scotia, Canada

<sup>9</sup>Department of Energy, Environmental & Chemical Engineering, Washington University in St. Louis, St Louis, MO, USA

<sup>10</sup>State Key Laboratory of Organic Geochemistry, Guangzhou Institute of Geochemistry, Chinese Academy of Science (CAS), Guangzhou, China

<sup>11</sup>Department of Chemistry and CIRES, University of Colorado Boulder, Boulder, CO, USA

<sup>12</sup>School of Physics and Astronomy, University of Leicester, Leicester, LE1 7RH, UK

<sup>13</sup>Atmospheric Research & Analysis, Inc., Cary, NC, USA

\*Correspondence to: Yiqi Zheng ([yzheng4@alaska.edu](mailto:yzheng4@alaska.edu)) and Jingqiu Mao ([jmao2@alaska.edu](mailto:jmao2@alaska.edu))

**Keywords:** Secondary organic aerosol; IEPOX; isoprene; coating; aerosol acidity.



## 1 Abstract

2 Organic aerosol (OA), with a large biogenic fraction in summertime southeast US, adversely  
3 impacts on air quality and human health. Stringent air quality controls have recently reduced  
4 anthropogenic pollutants including sulfate, whose impact on OA remains unclear. Three filter  
5 measurement networks provide long-term constraints on the sensitivity of OA to changes in  
6 inorganic species, including sulfate and ammonia. The 2000-2013 summertime OA decreases by  
7 1.7~1.9%/year with little month-to-month variability, while sulfate declines rapidly with  
8 significant monthly difference in early 2000s. In contrast, modeled OA from a chemical-  
9 transport model (GEOS-Chem) decreases by 4.9%/year with much larger monthly variability,  
10 largely due to the predominant role of acid-catalyzed reactive uptake of epoxydiols (IEPOX)  
11 onto sulfate. The overestimated modeled OA dependence on sulfate can be improved by  
12 implementing a coating effect and assuming constant aerosol acidity, suggesting the needs to  
13 revisit IEPOX reactive uptake in current models. Our work highlights the importance of  
14 secondary OA formation pathways that are weakly dependent on inorganic aerosol in a region  
15 that is heavily influenced by both biogenic and anthropogenic emissions.  
16  
17



## 18    1. Introduction

19    Organic aerosol (OA) accounts for a large fraction of ambient fine particulate matter mass,  
20    which strongly affects air quality, regional climate, and human welfare (Jimenez et al., 2009).  
21    Since the implementation of the Clean Air Act Amendments of 1990, there has been a significant  
22    decline in ambient aerosol in the United States, mostly due to reductions in inorganic aerosol  
23    mass following changes in emissions of sulfur dioxide ( $\text{SO}_2$ ), nitrogen oxides ( $\text{NO}_x = \text{NO} + \text{NO}_2$ ),  
24    as well as reductions in black carbon (EPA, 2011), leaving OA as the major component of fine  
25    particulate matter (50~70%) over the southeast US, especially in summer (Attwood et al., 2014;  
26    Kim et al., 2015). OA can be directly emitted by combustion processes (primary organic aerosol,  
27    POA) or secondarily formed (SOA) from the atmospheric oxidation of biogenic volatile organic  
28    compounds (BVOCs), mainly isoprene and monoterpenes, and also precursors from  
29    anthropogenic sources and biomass burning (Hayes et al., 2015; Hodshire et al., 2019). OA has  
30    also been declining across much of the US over the past few decades, primarily due to decreased  
31    anthropogenic emissions from vehicle and residential fuel-burning, except for the southeast US  
32    (Ridley et al., 2018). The southeast US is one of the largest BVOC emission hotspots in the  
33    world (Guenther et al., 2006), and at the same time is heavily populated with large anthropogenic  
34    emissions of pollutants. Biogenic SOA may account for 60-100% of OA in summertime  
35    southeast US (Kim et al., 2015; Xu et al., 2015b). To what extent biogenic SOA could be  
36    mediated through emission control strategies remains an open question (Carlton et al., 2010;  
37    Mao et al., 2018).  
38  
39    The oxidation of BVOCs produces hundreds of intermediate products. Some products have low  
40    volatility that can partition onto the condensed phase, while some gas-phase products can react in



41 the aqueous phase to form SOA. SOA formed from uptake of isoprene epoxydiols (IEPOX-  
42 SOA) (Paulot et al., 2009) appears to be the major confirmed aqueous SOA product globally,  
43 being important in all high isoprene and lower NO regions (Hu et al., 2015), along with glyoxal  
44 formed from isoprene and aromatics (Fu et al., 2008). Formation of SOA in clouds was  
45 investigated in the southeast US and found to be not statistically significant (Wagner et al.,  
46 2015). These pathways have been implemented into 3-dimensional global atmospheric chemistry  
47 and climate models using two different approaches. First, to simulate the partitioning of organic  
48 vapors, the BVOC oxidation products can be grouped based on their volatility (Volatility Basis  
49 Set, VBS), and the product yields and vapor pressures are parameterized for each surrogate  
50 precursor (Donahue et al., 2006; Pankow, 1994). Such empirical VBS schemes are usually  
51 derived using dry laboratory chamber experiments (with relative humidity RH<10%) and do not  
52 explicitly depend on aerosol water, RH, or inorganic aerosol mass or composition. Therefore,  
53 here we refer to the SOA formed through partitioning calculated by VBS as dry SOA. Second, a  
54 more explicit representation of aqueous SOA formation from isoprene products has been used  
55 recently, which incorporates dependence on inorganic aerosol volume and aerosol acidity  
56 (Budisulistiorini et al., 2017; Ervens et al., 2011; Fu et al., 2008; Marais et al., 2016; Pye et al.,  
57 2013). The relative contribution of dry versus aqueous SOA to total OA mass in the atmosphere  
58 is uncertain and has limited observational constraints.

59

60 Long-term field measurements show a decreasing trend of OA in the southeast US (Attwood et  
61 al., 2014; Hidy et al., 2014; Kim et al., 2015), which is likely linked to reductions in  
62 anthropogenic POA and SOA (Blanchard et al., 2016; Ridley et al., 2018), sulfate (Blanchard et  
63 al., 2016; Malm et al., 2017; Marais et al., 2017; Xu et al., 2015b, 2016) and NO<sub>x</sub> (Carlton et al.,



64 2010; Pye et al., 2010, 2019a; Xu et al., 2015b). The influence of sulfate on OA is thought to be  
65 mainly due to its influence on the uptake of isoprene gas-phase oxidation products, which are  
66 often small molecules that cannot directly condense due to high vapor pressure, but may undergo  
67 aqueous-phase reactive uptake onto wet sulfate particles to form aqueous SOA, as suggested by  
68 extensive laboratory and field studies (Budisulistiorini et al., 2015; Hu et al., 2015; Li et al.,  
69 2016; Liggio et al., 2005; McNeill et al., 2012; Riedel et al., 2016; Shrivastava et al., 2017;  
70 Surratt et al., 2010; Tan et al., 2012; Xu et al., 2016, 2015b). NO<sub>x</sub> plays a complex role in  
71 regulating oxidation capacity and different oxidation pathways (Kiendler-Scharr et al., 2016;  
72 Kroll et al., 2005, 2006; Li et al., 2018; Ng et al., 2017; Presto et al., 2005; Shrivastava et al.,  
73 2019; Zheng et al., 2015; Ziemann and Atkinson, 2012). Prior 3-D modeling studies with  
74 different SOA mechanisms provide different explanations for the long-term OA trend observed  
75 in the southeast US. For example, the dry SOA calculated by VBS framework with NO<sub>x</sub>-  
76 dependent yields implies a small decrease in OA following the reductions of NO<sub>x</sub> (Pye et al.,  
77 2013; Zheng et al., 2015), but has little dependence on changes in inorganic aerosol mass such as  
78 sulfate. On the other hand, models using aqueous SOA formation from isoprene attributed the  
79 decreasing OA from 1991 to 2013 to reductions in sulfate (Marais et al., 2017) but showed  
80 greater interannual variability than was observed. The driving mechanism for the OA trend in the  
81 southeast US remains to be elucidated.

82

83 Here we use observations from three surface filter-based networks (IMPROVE, SEARCH,  
84 CSN), combined with a 3-dimensional chemical transport model GEOS-Chem v12.1.0, to  
85 examine the long-term trend and more importantly, the month-to-month variability of OA in the



86 southeast US during 2000-2013. The results provide new observational constraints on the drivers  
87 of OA variability and the SOA formation mechanisms in the southeast US.

88

89 **2. Methods**

90 **2.1 Observational datasets.**

91 We use surface filter-based measurement of fine particulate matter mass and composition  
92 (including organic carbon, OC) in 2000-2013 from three networks: the Interagency Monitoring  
93 of Protected Visual Environments (IMPROVE) (Solomon et al., 2014), the SouthEastern Aerosol  
94 Research and Characterization (SEARCH) (Edgerton et al., 2005), and the Environmental  
95 Protection Agency's PM<sub>2.5</sub> National Chemical Speciation Network (CSN) (Solomon et al.,  
96 2014). We select 21 IMPROVE sites, 3 SEARCH rural sites and 36 CSN sites within the  
97 southeast US region [29°~37°N, 74°~96°W] (Figure S1). The SEARCH sites are organized in  
98 rural/urban pairs (Edgerton et al., 2005) and only the data from the rural sites are used here to  
99 represent background conditions. IMPROVE sites are mostly rural (Solomon et al., 2014). The  
100 OC measurement in the CSN network in 2004-2009 gradually shifted to a different protocol and  
101 analytical technique than the early 2000s, which led to the discontinuity in long-term trend  
102 (Figure S2), therefore we only use CSN data to examine the monthly variability of OA, and  
103 focus on IMPROVE and SEARCH for all analysis. The 3-day OC measurement from IMPROVE  
104 and daily OC from SEARCH and CSN are averaged to monthly values. A factor of 2.1 is used to  
105 convert measured organic carbon (OC) to organic aerosol mass, as suggested by the southeast  
106 US field measurements (Pye et al., 2017; Schroder et al., 2018).

107



108 We use OA measurements by Aerosol Mass Spectrometer (AMS) from the Southern Oxidant  
109 and Aerosol Studies campaign (SOAS) at the Centerville, AL Site in 06/01/2013-07/15/2013  
110 (SOAS2013). The OA measurements and derived IEPOX-SOA factor calculated by Positive  
111 Matrix Factorization (PMF) analysis (Hu et al., 2015; Xu et al., 2015a, 2018) are from two  
112 independent groups: one group from Georgia Institute of Technology led by Prof. Nag Lee Ng,  
113 the other from University of Colorado Boulder led by Prof. Jose L. Jimenez, denoted as Obs\_GT  
114 and Obs\_CU, respectively.

115

116 **2.2 Modeling framework**

117 **2.2.1 GEOS-Chem**

118 In this study we use the 3-dimensional global chemical transport model GEOS-Chem version  
119 12.1.1 ([DOI: 10.5281/zenodo.2249246](https://doi.org/10.5281/zenodo.2249246), <https://github.com/geoschem/>) with detailed O<sub>3</sub>-NO<sub>x</sub>-  
120 HO<sub>x</sub>-CO-VOC-aerosol tropospheric chemistry (Bey et al., 2001; Mao et al., 2013). Isoprene  
121 chemistry is described in (Fisher et al., 2016; Travis et al., 2016). GEOS-Chem is driven by  
122 offline meteorology 1999-2013 from the NASA Modern-Era Retrospective analysis for Research  
123 and Applications, version 2 (MERRA-2 <https://gmao.gsfc.nasa.gov/reanalysis/MERRA-2/>). The  
124 global anthropogenic emissions are from the Community Emissions Data System (CEDS)  
125 inventory, with the US region replaced by the EPA's National Emission Inventory for 2011  
126 (NEI11v1). The monthly mean anthropogenic emissions of CO, SO<sub>2</sub>, NO<sub>x</sub>, NH<sub>3</sub>, VOCs, OC and  
127 black carbon are mapped over 0.1°×0.1° and scaled to the year 2011 by the ratio of national  
128 annual totals from 2000 to 2013 (Travis et al., 2016). Biomass burning emissions are from  
129 Global Fire Emissions Database version 4 (GFED4) (Randerson et al., 2015). Biogenic  
130 emissions of isoprene and terpenes are online calculated by the Model of Emissions of Gases and



131      Aerosols from Nature (MEGAN2.1) (Guenther et al., 2012) that is also driven by MERRA-2  
132      meteorology.

133

134      For organic aerosol, we employ the complexSOA scheme for SOA modeling for all simulations  
135      in this study (Marais et al., 2016; Pye et al., 2010). POA are regarded as nonvolatile. This SOA  
136      modeling includes a 4-product Volatility-Basis-Set (VBS) for SOA formation from reversible  
137      condensation of oxidation products of biogenic terpenes (including monoterpenes and  
138      sesquiterpenes), and anthropogenic VOCs, referred to as terpene-SOA and anthropogenic SOA,  
139      respectively. The SOA calculated through VBS parameterization is fitted based on dry chamber  
140      (RH<10%) results independent of inorganic aerosol, aerosol water and RH (Pye et al., 2010).

141      The complexSOA scheme also includes aqueous SOA formed from reactive uptake of isoprene  
142      oxidation products, including IEPOX, glyoxal, C<sub>4</sub> epoxides, methylglyoxal, non-IEPOX product  
143      of the ISOOPOOH oxidation and hydroxynitrates from NO<sub>3</sub>-initiated oxidation (Marais et al.,  
144      2016). The sulfate-nitrate-ammonium aerosol thermodynamics including aerosol acidity is  
145      computed with the ISORROPIA II thermodynamic model (Fountoukis and Nenes, 2007; Pye et  
146      al., 2009; Song et al., 2018).

147

148      We run the GEOS-Chem model at 4°×5° latitude by longitude continuously from 10/01/1999 to  
149      12/31/2013. For each year, the restart file at 05/01 from the continuous 4°×5° simulation has  
150      been regredded to 2°×2.5° and is used to initiate 2°×2.5° simulations from 05/01 to 08/31 each  
151      year. The 2°×2.5° simulations are adequate when modeling continental boundary layer chemistry  
152      (Yu et al., 2016). The May results are discarded as spin-up and the results of June, July and  
153      August are used for analysis. We do four sets of 2°×2.5° simulations: Default (using default



154 complexSOA scheme); CT (with coating effect for IEPOX reactive uptake); CT\_newNH<sub>3</sub> (with  
155 coating effect and US NH<sub>3</sub> emissions replaced by satellite-derived NH<sub>3</sub> inventory); CT\_H01  
156 (with coating effect and fixing aerosol a<sub>H+</sub> at 0.1 mol/L when calculating IEPOX reactive  
157 uptake).

158

159 **2.2.2 Coating**

160 The default IEPOX-SOA mechanism in GEOS-Chem uses aerosol-phase reaction rates from  
161 laboratory chamber studies with pure acidic inorganic particles (Gaston et al., 2014; Riedel et al.,  
162 2015), and a representative effective Henry's law constant obtained by matching the model to the  
163 observations at SOAS2013 campaign, to estimate the reactive uptake coefficient  $\gamma_{IEPOX}$ . In the  
164 default scheme,  $\gamma_{IEPOX}$  is calculated as follows:

$$165 \frac{1}{\gamma_{IEPOX}} = \frac{R_p \omega}{4D_g} + \frac{1}{\alpha} + \frac{1}{\Gamma_{aq}}$$

$$166 \Gamma_{aq} = \frac{4VRTH_{aq}k_{aq}}{S_a \omega}$$

167 Where  $R_p$  is the particle radius of the inorganic sulfate-nitrate-ammonium particle (cm),  $\omega$  is the  
168 mean molecular speed (cm/s),  $D_g$  is the gas-phase diffusion coefficient (0.1 cm<sup>2</sup>/s),  $\alpha$  is the mass  
169 accommodation coefficient ( $\alpha=0.1$ ),  $S_a$  is the total (wet) particle surface area (cm<sup>2</sup>/cm<sup>3</sup>),  $V$  is the  
170 total (wet) particle volume (cm<sup>3</sup>/cm<sup>3</sup>),  $R$  is the ideal gas constant (L atm/mol/K),  $T$  is temperature  
171 (K),  $H_{aq}$  is the Henry's law coefficient ( $1.7 \times 10^7$  M/atm), and  $k_{aq}$  is the first-order reaction rate  
172 constant (s<sup>-1</sup>):

$$173 k_{aq} = k_{H^+}[H^+] + k_{nuc}[nuc]a_{H^+} + k_{ga}[ga]$$



174 where  $k_{H^+}$  ( $=0.036 \text{ M}^{-1}\text{s}^{-1}$ ),  $k_{nuc}$  ( $=2 \times 10^{-4} \text{ M}^{-1}\text{s}^{-1}$ ) and  $k_{ga}$  ( $=7.3 \times 10^{-4} \text{ M}^{-1}\text{s}^{-1}$ ) are the reaction  
175 rates due to acid-catalyzed ring-opening, presence of nucleophiles (including nitrate and sulfate)  
176 and presence of bisulfate acids, respectively (Gaston et al., 2014; Marais et al., 2016).

177

178 We implement a linear coating effect for the IEPOX-SOA formation. The coating effect is fitted  
179 using laboratory-derived values of  $\gamma_{IEPOX}$  on particles containing both ammonium bisulfate and  
180 ethylene glycol under RH=50% conditions (Gaston et al., 2014). In the coating scheme,  $\gamma'_{IEPOX}$   
181 is calculated as above with  $R_p$ ,  $V$  and  $S_a$  updated considering OA coated outside the inorganic  
182 core. Then, the fitted function is applied to modify  $\gamma'_{IEPOX}$ :

183 
$$\gamma_{IEPOX\_modified} = \gamma'_{IEPOX} \times (1 - 1.3 \times \chi_{org})$$

184 where  $\chi_{org}$  is the mass fraction of OA in the mixed particle including both the inorganic aerosol  
185 and OA. When  $\chi_{org}>0.7$ , the IEPOX uptake will be terminated, i.e.  $\gamma_{IEPOX\_modified} = 0$ . We  
186 assume all OA is coated outside the inorganic aerosol core when calculating the IEPOX reactive  
187 uptake. The increased particle radius  $R_p$  and surface area  $S_a$  of the mixed particle will partially  
188 offset the impact of reduced reaction probability  $\gamma_{IEPOX\_modified}$ , consistent with another study  
189 (Jo et al., 2019).

190

### 191 **2.2.3 Satellite-derived NH<sub>3</sub> emissions**

192 We use the Cross-track Infrared Sounder (CrIS) satellite-derived NH<sub>3</sub> emissions in a sensitivity  
193 test in this study. The top-down monthly NH<sub>3</sub> emissions over the contiguous US at  $0.25^\circ \times$   
194  $0.3125^\circ$  latitude by longitude are derived from CrIS v1.5 measurements of NH<sub>3</sub> profiles  
195 (Shephard and Cady-Pereira, 2015) for the year 2014 through a 4D-Var approach using GEOS-  
196 Chem and its adjoint model (Henze et al., 2007). The CrIS-derived emissions are then regridded



197 to  $0.1^\circ \times 0.1^\circ$  to replace the default NEI11 emissions for the year 2011 and applied the same  
198 annual scaling factors for 2000-2013. There is no significant trend from 2000 to 2013 (Figure  
199 S3), consistent with other studies suggesting nearly constant NH<sub>3</sub> emissions from 2001 to 2014  
200 (Butler et al., 2016). The CrIS-derived emissions used the HTAPv2 emissions inventory as the  
201 prior emissions, which is based on the 2008 NEI emissions over the US (Janssens-Maenhout et  
202 al., 2015). The top-down annual mean emissions are ~52% higher than the prior emissions, likely  
203 because the prior emissions underestimate agricultural emissions, in particular springtime  
204 fertilizer and livestock sources over the Central US. Meanwhile, some smaller values then the  
205 prior emissions were found in the Central Valley, southern Minnesota, northern Iowa and  
206 southeast North Carolina during warm months. Using the top-down emissions in GEOS-Chem  
207 increases the correlation coefficient ( $r$ ) between modeled monthly mean NH<sub>3</sub> and surface  
208 observations from 0.74 to 0.93 and reduces the normalized mean bias of domain-averaged annual  
209 mean simulated NH<sub>3</sub> by a factor of 1.9. The seasonal cycle of simulated wet NH<sub>4</sub><sup>+</sup> is also  
210 improved ( $r$  increased from 0.70 to 0.86), but the normalized mean bias of domain-averaged  
211 annual simulated wet NH<sub>4</sub><sup>+</sup> increases from 0.34 to 0.96 due to overly strong wet scavenging in  
212 the model. The latter issue was ultimately resolved in Cao et al. (submitted) and the final top-  
213 down emissions reported therein differ from those reported here; nevertheless, the emissions  
214 estimates used here provide a valuable basis for conducting a sensitivity experiment.  
215

### 216 **2.3 Multivariate linear regression analysis**

217 In this study we did a multivariate regression analysis of monthly IEPOX-SOA ( $\mu\text{g}/\text{m}^3$ ) against  
218 sulfate aerosol ( $\mu\text{g}/\text{m}^3$ ), aerosol acidity  $a_{\text{H}^+}$  (mol/L) and isoprene emission ( $ISOP_{\text{emis}}$  mg/m<sup>2</sup>/hr):

$$219 IEPOX-SOA = \beta_1 \times \text{sulfate} + \beta_2 \times a_{\text{H}^+} + \beta_3 \times ISOP_{\text{emis}} + b$$



220 Mean values have been subtracted from all variables, which are then divided by standard  
221 deviations.  $\beta_1$ ,  $\beta_2$  and  $\beta_3$  are standardized partial regression coefficients associated with sulfate  
222 aerosol,  $a_{H^+}$  and isoprene emission, and can be directly compared to evaluate the relative  
223 importance of the three variables. We apply the regression analysis using monthly data within  
224 different time frames (2000-2013, 2000-2004, 2005-2008 and 2009-2013 as in Table S1) to  
225 determine the evolving importance of variables.

226

227

### 228 **3. Results**

#### 229 **3.1 Long-term trend and month-to-month variability (MMV) of OA**

230 In the southeast US, observations from the IMPROVE and SEARCH network both show a  
231 reduction in summertime surface OA concentration from 2000 to 2013 (Figure 1). Observational  
232 results are averaged using 21 IMPROVE sites and 3 SEARCH sites within the southeast US. OA  
233 concentration averaged over June-July-August (JJA) 2000-2013 is  $4.2 \mu\text{g}/\text{m}^3$  from the  
234 IMPROVE sites, and  $5.7 \mu\text{g}/\text{m}^3$  from SEARCH sites. A similar ~30% summertime low bias on  
235 the IMPROVE sites was documented by Kim et al. (2015) compared to the SEARCH sites,  
236 which is thought to be due to evaporation of OA from the filters after collection, as the  
237 IMPROVE filters stay several days on site after sampling and are shipped without refrigeration,  
238 while the SEARCH filters are analyzed in-situ. Despite different magnitudes, OA from the two  
239 networks demonstrate similar trends and interannual variability. The 2000-2013 trend of JJA OA  
240 mass is -1.7%/year for IMPROVE and -1.9%/year for SEARCH. Compared to the slow decrease  
241 in OA, a faster declining trend is found for sulfate from IMPROVE (-6.9%/year) and SEARCH  
242 (-6.7%/year) for the same period.



243

244 Compared to the observations, the default GEOS-Chem model predicts a steeper decreasing  
245 trend of OA mass during 2000-2013 (Figure 1). Modeling results are averaged over the domain  
246 [29°~37°N, 74°~96°W] excluding ocean grid cells (Figure S1). The 2000-2013 JJA-averaged  
247 OA from the default model is 6.7  $\mu\text{g}/\text{m}^3$ , higher than OA from IMPROVE and SEARCH.  
248 Modeled total OA mass decreases at a rate of 4.9%/year, about 1.9 (1.6) times faster than  
249 IMPROVE (SEARCH) OA (student's t-test  $p<0.001$ ). The strong reduction in total OA mass is  
250 dominated by aqueous SOA, especially through reactive uptake of IEPOX, with no decreasing  
251 trend in other components (Figure 1). The contribution of IEPOX-SOA to total OA mass  
252 decreases from 61% in the early 2000s to 28% in 2013.

253

254 A main constraint comes from the MMV of OA in the southeast US. IMPROVE and SEARCH  
255 OA observations show little variability among June, July and August, despite large MMV of  
256 sulfate in early 2000s (Figure 2A). We find similar behavior from another observation network,  
257 CSN. The discontinuity in OA trend in the CSN network is due to different protocols applied  
258 (Figure S2). Within sites using the same protocol, there are no systematic monthly differences,  
259 which agrees with IMPROVE and SEARCH. In contrast, modeled OA displays large MMV  
260 between June, July and August from 2000 to 2008, where OA in July and August is 1~3 times of  
261 June values (Figure 2A). Such large MMV is dominated by aqueous SOA, especially from the  
262 reactive uptake of IEPOX. Prior to 2008, the simulated IEPOX-SOA alone can be up to a factor  
263 2 higher than the observed total OA (Figure 2). The other components including POA and dry  
264 SOA (including terpene-SOA and Anthropogenic SOA) formed through partitioning together  
265 have low concentrations and small MMV. The default model well captures the variability of



266 observed sulfate (Figure 2A), with an average of  $3.8 \mu\text{g}/\text{m}^3$  and a trend of -6.9%/year, as  
267 compared to -6.9%/year (average concentration  $4.2 \mu\text{g}/\text{m}^3$ ) from IMPROVE and -6.7%/year  
268 (average concentration  $4.3 \mu\text{g}/\text{m}^3$ ) from SEARCH.

269

270 The large MMV in the model suggests a much stronger modeled OA dependence on sulfate than  
271 observations. In 2000-2004, changes in modeled sulfate from June to July and/or August  
272 correspond to large MMV of modeled OA mass. In contrast, little MMV is found in observed  
273 OA mass during the same months despite large MMV in observed sulfate (Figure 2A). From a  
274 linear regression analysis using all monthly data in 2000-2013, the OA-to-sulfate regression  
275 slope is  $m=0.29$  ( $r^2=0.25$ ) from IMPROVE,  $m=0.51$  ( $r^2=0.43$ ) from SEARCH, and  $m=1.87$   
276 ( $r^2=0.57$ ) from the default model, even though the default model well captures the magnitude,  
277 trend, and monthly variability of observed sulfate. In summary, simulated total OA mass in the  
278 standard GEOS-Chem model, dominated by IEPOX-SOA, has a steeper decreasing trend from  
279 2000 to 2013 than the observations, and has a large MMV indicating strong dependence on  
280 sulfate.

281

### 282 **3.2 What controls the modeled IEPOX-SOA variability?**

283 The strong dependence of IEPOX-SOA on sulfate is well-established by laboratory and field  
284 work: wet sulfate particles provide the surface and volume of liquid media for IEPOX reactive  
285 uptake (Budisulistiorini et al., 2017; Eddingsaas et al., 2010; Riva et al., 2016; Xu et al., 2015b,  
286 2016), and serve as nucleophiles for nucleophilic addition to form organosulfates (Nguyen et al.,  
287 2014; Surratt et al., 2007b). Sulfate ( $\text{SO}_4^{2-}$ ), together with ammonium ( $\text{NH}_4^+$ ), nitrate ( $\text{NO}_3^-$ ) and  
288 other ions, regulates proton ( $\text{H}^+$ ) activity ( $a_{\text{H}^+}$ ) that can catalyze the ring-opening of epoxide



289 group leading to the formation of IEPOX-SOA (Gaston et al., 2014; Pye et al., 2013; Surratt et  
290 al., 2007a). However, some recent studies suggest that IEPOX-SOA is not well correlated with  
291 aerosol acidity estimated from thermodynamic models (Budisulistiorini et al., 2015; Lin et al.,  
292 2013; Xu et al., 2015b), although the lack of direct measurements of aerosol acidity may be a  
293 limitation. We use the GEOS-Chem model here to examine the simulated IEPOX-SOA  
294 dependence on sulfate, aerosol acidity, and emissions of isoprene which produce IEPOX at high  
295 yields under low-NO<sub>x</sub> conditions (Paulot et al., 2009). We do not treat aerosol water as an  
296 independent driver because the dilution effect of aerosol water is implicitly considered in the  
297 inorganic sulfate-ammonium-nitrate aerosol volume and acidity calculation, and studies have  
298 shown that particle water is not a limiting factor unless the particle is purely dry (Nguyen et al.,  
299 2014; Riva et al., 2016; Xu et al., 2015b) which is rare in summertime in the southeast US.  
300

301 We find that the large MMV of OA in the model is mainly driven by sulfate concentrations and  
302 aerosol acidity (Figure 3). Prior to 2008, IEPOX-SOA production is largely enhanced by  
303 abundant sulfate (Gaston et al., 2014). Due to this high level of sulfate (about >4 µg/m<sup>3</sup>), the  
304 modeled aerosol acidity becomes particularly sensitive to variations in NH<sub>3</sub> emissions. For the  
305 default model setup, we use monthly anthropogenic emissions from the EPA's National  
306 Emissions Inventory 2011 (NEI11v1) in the US and adjust to each year from 2000 to 2013 using  
307 national annual scaling factors (Travis et al., 2016), which suggests no significant long-term  
308 trend of NH<sub>3</sub> emissions from 2000 to 2013 (Figure S3). The NH<sub>3</sub> emissions in August are about  
309 25% lower than in June and July (Figure S3). As a result, the  $a_{H^+}$  in August is up to 3 times  
310 higher than June, leading to high production of IEPOX-SOA in August. Both sulfate and aerosol  
311 acidity appear to be the dominant contributors to MMV of OA during this period. After 2008,



312 IEPOX-SOA formation is substantially suppressed, due to small SO<sub>2</sub> emissions and low modeled  
313 aerosol acidity  $a_{H^+}$  with small monthly variability. Isoprene emissions also contribute to the  
314 month-to-month and interannual OA variability in the model.

315

316 The multivariate linear regression analysis of IEPOX-SOA quantitatively determines the relative  
317 importance of its three drivers in the model. Using all monthly data in 2000-2013, the  
318 standardized regression coefficients ( $\beta$ ) associated with  $a_{H^+}$ , sulfate aerosol concentration and  
319 isoprene emission are  $\beta=0.50$  ( $r^2=0.71$ ),  $\beta=0.39$  ( $r^2=0.64$ ) and  $\beta=0.34$  ( $r^2=0.18$ ), respectively,  
320 suggesting that aerosol acidity is the dominant controlling factor. The three variables together  
321 explain 88% of the variability of IEPOX-SOA. Their relative importance changes over time  
322 (Table S1). Aerosol acidity strongly correlates with IEPOX-SOA in 2005-2008 ( $\beta=0.57$ ,  
323  $r^2=0.82$ ) but its role becomes much weaker after 2008 ( $\beta=0.27$ ,  $r^2=0.56$ ). Sulfate aerosol is  
324 always the first or second most important driver, especially in 2000-2004 ( $\beta=0.46$ ,  $r^2=0.76$ ).  
325 Isoprene emission contributes to the overall interannual variability, for example leading to the  
326 relatively low IEPOX-SOA in 2003-2004 and the peak in 2011 (Figure 3).

327

### 328 **3.3 Narrowing the gap between model and observation**

#### 329 **3.3.1 Coating**

330 Several reasons may lead to the large monthly variations of the modeled OA. The modeled  
331 IEPOX-SOA shows a much stronger sensitivity to aerosol acidity than suggested by field  
332 observations, which found weak or no correlation between observed IEPOX-SOA and derived  
333 aerosol acidity (Budisulistiorini et al., 2015; Lin et al., 2013; Worton et al., 2013; Xu et al.,  
334 2015b). Lack of consideration of organic coating effect may provide one possible explanation. In



335 the real atmosphere, inorganic aerosol is generally internally mixed with other organics (Anttila  
336 et al., 2006; Murphy et al., 2006). The presence of an organic coating may alter the solubility and  
337 diffusion properties at the surface of inorganic particles and diminish further uptake of IEPOX.  
338 By implementing a linear coating effect for the IEPOX uptake, both the magnitude of  $\gamma_{IEPOX}$  and  
339 its sensitivity to acidity have been reduced. Figure 4A shows a schematic illustrating the  
340 dependence of the  $\gamma_{IEPOX}$  coating effect on acidity  $a_{H^+}$  and organic mass fraction ( $\chi_{org}$ ). The  
341 original  $\gamma_{IEPOX}$  without coating is represented at  $\chi_{org}=0$ . The orange line in Figure 4A shows the  
342 approximate position of JJA-averaged acidity and organic mass fraction in the model simulation  
343 with coating effect (simulation name: ‘CT’). Adding a coating reduces  $\gamma_{IEPOX}$  by almost half, but  
344 the impact on the total reactive uptake rate of IEPOX is partially compensated by the  
345 corresponding increase in particle surface area. The sensitivity of  $\gamma_{IEPOX}$  to acidity has also been  
346 reduced especially during the early 2000s (Figure 4A). The CT simulation reduces the southeast  
347 US JJA-averaged IEPOX-SOA concentrations by 0.3~1.8  $\mu\text{g}/\text{m}^3$  (Figure 4C).  
348

### 349 **3.3.2 NH<sub>3</sub> emissions and aerosol acidity**

350 Second, recent studies present contradictory results and explanations on the long-term trend of  
351 aerosol acidity in the southeast US (Pye et al., 2019b; Silvern et al., 2017; Weber et al., 2016). In  
352 this study, we show that the decreasing trend of aerosol acidity from the standard GEOS-Chem  
353 model is mainly caused by high acidity in August before 2008, which corresponds to insufficient  
354 NH<sub>3</sub> emissions in high sulfate environments. The NEI11v1 inventory is used in the default  
355 configuration, in which NH<sub>3</sub> emissions in June and July are 30% higher than in August (Figure  
356 S3), but not all NH<sub>3</sub> emission inventories agree with such pattern (Paulot et al., 2014). We did a  
357 sensitivity test replacing the default US NH<sub>3</sub> emissions from NEI11v1 by a new NH<sub>3</sub> emission



358 product derived from CrIS satellite observations, which has higher emissions and smaller MMV  
359 among June, July and August (Figure S3). In the simulation with updated NH<sub>3</sub> emissions in the  
360 US from 2000 to 2013 ('CT\_newNH<sub>3</sub>'), the resulting simulated aerosol acidity is substantially  
361 changed in 2000-2008 (Figure 4B). The high acidity ( $a_{H^+}=0.55\text{--}0.9 \text{ mol/L}$ ) in August has been  
362 reduced to around 0.2 mol/L and is much closer to June and July values (Figure 3B). The results  
363 suggest that the fine particles in the southeast US are within a regime where the acidity ( $a_{H^+}$  in  
364 units of mol/L) is sensitive to NH<sub>3</sub> emissions relative to sulfate concentration, though  
365 corresponding pH changes are small (pH within 0.5~1.5, Figure S3). Small changes in NH<sub>3</sub> may  
366 lead to large changes in  $a_{H^+}$  especially when sulfate concentrations are high, resulting in high  
367 month-to-month variability of the IEPOX uptake. After updating the NH<sub>3</sub> emissions using the  
368 satellite-based estimates, the model simulates a much more stable trend in aerosol acidity from  
369 2000 to 2013 (Figure 4B), consistent with recent thermodynamic modeling studies that suggested  
370 steady aerosol acidity despite large reductions in observed sulfate (Pye et al., 2019b; Weber et  
371 al., 2016).

372

373 Due to the high uncertainty associated with the derived NH<sub>3</sub> emission product and acidity  
374 calculation (Guo et al., 2015, 2018; Silvern et al., 2017; Song et al., 2018; Tao and Murphy,  
375 2019), we conducted another simulation 'CT\_H01' that fix  $a_{H^+}$  level at 0.1 mol/L when  
376 calculating IEPOX uptake rate, corresponding to the observed  $a_{H^+}$  value during the 2013 SOAS  
377 campaign (Weber et al., 2016). The two simulations, CT\_newNH<sub>3</sub> and CT\_H01, yield similar  
378 long-term trends of IEPOX-SOA in the southeast US (Figure S4). For the SOAS2013 campaign  
379 at Centerville, AL from 06/01/2013 to 07/15/2013, the CT\_H01 scheme simulates an average  
380 IEPOX-SOA concentration of 0.74 μg/m<sup>3</sup>, similar to 0.81 μg/m<sup>3</sup> in the default model, and agrees



381 well with the two independent Aerosol Mass Spectrometer measurements ( $0.97 \mu\text{g}/\text{m}^3$  from  
382 obs\_GT and  $0.68 \mu\text{g}/\text{m}^3$  from obs\_CU, see daily time series in Figure S5). The CT\_newNH<sub>3</sub>  
383 scheme simulates an average IEPOX-SOA concentration of  $0.34 \mu\text{g}/\text{m}^3$ , lower than the  
384 observation and the other models by a factor of >2, due to both the coating effect and small  
385 aerosol  $a_{H^+}$  values ( $a_{H^+} < 0.1 \text{ mol/L}$ , Figure 4B). In general, the fixed acidity in the CT\_H01  
386 simulation well captures the measured IEPOX-SOA from the SOAS2013 campaign (Figure S5),  
387 and improves the modeled total OA mass relative to the observations: The modeled long-term  
388 decreasing rate of JJA-average OA from 2000 to 2013 has been reduced from 4.9%/year to  
389 3.2%/year, better compared to the IMPROVE (1.7%/year) and SEARCH (1.9%/year)  
390 observations, but is still higher (Figure 4C). The modeled MMV of OA have also been greatly  
391 reduced (Figure 4D).

392

### 393 **3.3.3 Relationships between OA and sulfate**

394 The formation of aqueous SOA explicitly depends on sulfate aerosol and aerosol acidity which is  
395 also impacted by sulfate. The default model, in which a large fraction of simulated total OA mass  
396 is from aqueous SOA (mostly IEPOX-SOA), shows a stronger dependence of total OA on sulfate  
397 than the observations (Figure 5). The OA-to-sulfate regression slope calculated using monthly  
398 OA and sulfate (averaged from all sites beforehand for each network) is  $m=1.87$  for the default  
399 simulation, much higher than  $m=0.29$  from IMPROVE and  $m=0.51$  from SEARCH. Such strong  
400 dependence is clearly demonstrated by the MMV of IEPOX-SOA (Figure 2). Adding the  
401 coating effect and fixing  $a_{H^+}=0.1 \text{ mol/L}$  substantially reduces the MMV of IEPOX-SOA and the  
402 simulated monthly OA-to-sulfate slope ( $m=1.02$ ).

403



404 Despite the model improvement against the observations in terms of OA and IEPOX-SOA  
405 magnitude and long-term relationship with sulfate, the CT\_H01 scheme needs to be further  
406 improved. The rate of OA decreases per year in CT\_H01 is about 0.8 times higher than the long-  
407 term observations, with modeled MMV still larger than observations in early 2000s (Figure 4D).  
408 Recent studies (Riva et al., 2019) suggested that the IEPOX-SOA production per unit mass of  
409 sulfate likely increases with decreasing sulfate due to changes in aerosol properties, such as  
410 acidity, morphology, phase state and viscosity. Further modeling studies with separated IEPOX-  
411 SOA species and detailed aerosol properties are needed to achieve a better mechanistic  
412 understanding of the dependence of OA on inorganic aerosol.  
413

#### 414 **4. Summary and Discussion**

415 Significant reduction of SO<sub>2</sub> emissions, combined with monthly variations of sulfate and NH<sub>3</sub>  
416 emissions, provide a unique dataset to test the sensitivity of biogenic SOA formation to inorganic  
417 species. Observations from two networks (IMPROVE and SEARCH) show a slowly decreasing  
418 trend in total OA mass from 2000 to 2013 in the southeast US (-1.7%/year from IMPROVE and -  
419 1.9%/year from SEARCH), in contrast to a much faster rate of sulfate reduction (-6.9%/year  
420 from IMPROVE and -6.7%/year from SEARCH). The standard version of GEOS-Chem model  
421 was able to reproduce the long-term trend of sulfate (-6.7%/year), but with a faster decrease of  
422 OA (-4.9%/year) and larger interannual variability.  
423

424 The MMV of total OA mass during summers provides a novel observational constraint on SOA  
425 formation mechanism. Remarkably, we find little MMV of OA from all three surface networks  
426 (IMPROVE, SEARCH and CSN) during summer months in 2000-2013, despite larger MMV in



427 sulfate and NH<sub>3</sub> emissions. This is in contrast to the standard version of the GEOS-Chem model,  
428 which shows a much larger MMV of OA during 2000-2008. Large MMV of OA in the standard  
429 model is mainly due to the high sensitivity of modeled IEPOX-SOA to sulfate and aerosol  
430 acidity (and NH<sub>3</sub> emissions) when sulfate aerosol is abundant. The resulting strong correlation  
431 between OA and sulfate also appears to be at odds with long-term observations (Figure 5).  
432 Incorporating a coating effect for IEPOX uptake and fixing aerosol acidity, have together  
433 improved the model performance in terms of OA trend, variability and the relationship between  
434 OA and sulfate, though further improvement is needed.

435

436 There are many uncertainties associated with the calculation of IEPOX-SOA formation. In the  
437 default scheme, the Henry's law constant for IEPOX uptake was tuned using measurements from  
438 the SOAS2013 campaign and was found to be  $1.7 \times 10^7$  M/atm, 10 times smaller than suggested  
439 by Gaston et al. (2014) based on laboratory experiments. The default simulation agrees well with  
440 surface IEPOX-SOA data from SOAS2013 and SEAC4RS 2013 aircraft campaigns (Marais et  
441 al., 2016) but overestimates OA magnitude and MMV against long-term observations from  
442 IMPROVE and SEARCH. The CT\_newNH<sub>3</sub> simulation reproduces the long-term OA trend but  
443 underestimates IEPOX-SOA by a factor of 2 against SOAS 2013. The coating effect may be  
444 stronger than used here, as Gaston et al. (2014) used a low viscosity organic material in the  
445 experiments. The NH<sub>3</sub> emissions (which are critical for the calculation of aerosol acidity) are  
446 highly uncertain (Dammers et al., 2019), and the acidity calculation is further complicated by  
447 non-volatile cations (Guo et al., 2018) and meteorological conditions (Guo et al., 2015; Tao and  
448 Murphy, 2019). Uncertainties are also associated with the volatility of IEPOX-SOA. Some  
449 studies suggested a large fraction of IEPOX-SOA compounds (e.g. 2-methyltetrool) are semi-



450 volatile and can re-evaporate back into gas-phase (Ambro et al., 2019; Isaacman-VanWertz et  
451 al., 2016), while other studies suggest IEPOX-SOA products are mostly nonvolatile or low  
452 volatility (Hu et al., 2016; Lopez-Hilfiker et al., 2016). As multiple parameters may be tuned in  
453 the model to fit observations, further laboratory, field and modeling studies are needed to  
454 integrate Henry's law constant, IEPOX-SOA yields, volatility, coating effect and acidity  
455 dependence for a better mechanistic understanding. The CT\_H01 scheme lacks mechanical  
456 representation of detailed aerosol properties like phase state, acidity, viscosity and morphology,  
457 but reasonably captures both the OA and IEPOX-SOA magnitude (compared to both the three  
458 filter measurement networks and the SOAS2013 campaign), long-term variability and  
459 relationship with sulfate (Figure 4, 5, S5), therefore may serve as a simplified representation for  
460 climate models. For all kinds of models, long-term filter-based measurements, especially  
461 intraseasonal MMV, are important observational constraints that should be considered in model  
462 development.

463

464 Even with our improved model, the rate of OA decrease per year is still 0.8 times higher the  
465 long-term observations, and still shows a higher MMV than observations particularly in early  
466 2000s (Figure 4D). Such discrepancies may suggest a more important role of SOA pathways that  
467 are less dependent on inorganic aerosol, such as the gas-aerosol partitioning. Despite a large  
468 MMV in IEPOX-SOA, Xu et al. (2015a) finds the less-oxidized oxygenated OA (LO-OOA, an  
469 indicator for freshly-formed monoterpene SOA) and the more-oxidized oxygenated OA (MO-  
470 OOA, also likely from biogenic sources) with little MMV in summer months, and they  
471 contribute to more than 50% of total OA mass in the southeast US (Xu et al., 2018). The  
472 important role of monoterpenes SOA is also confirmed by molecular level characterization of



473 organic aerosols (Zhang et al., 2018). Other pathways may contribute to SOA to some extent and  
474 may add to the predicted SOA formed by partitioning, including biogenic SOA from auto-  
475 oxidation (Bianchi et al., 2019; Pye et al., 2019a), in-cloud SOA formation that may be less  
476 dependent on acidity than aqueous SOA (Tsui et al., 2019), a small but underestimated  
477 contribution of anthropogenic SOA (Schroder et al., 2018; Shah et al., 2019), and other possible  
478 mechanisms (Schwantes et al., 2019). Further quantifying the relative importance of the different  
479 pathways will allow a more accurate quantification of the anthropogenic influence on biogenic  
480 SOA and the associated radiative forcing.

481

482



483

### 484 **Data availability**

485 The observational datasets from long-term filter measurement networks IMPROVE and CSN are  
486 available at <http://views.cira.colostate.edu/fed/QueryWizard/Default.aspx>. The SEARCH  
487 observational datasets are available by contacting E. Edgerton. The model code and modeling  
488 results are available by contacting Y. Zheng and J. Mao.

489

### 490 **Acknowledgement**

491 YZ and JM acknowledge funding from NOAA NA18OAR4310114. HC and DKJ recognize  
492 support from NASA 80NSSC18K0689. WH and JLJ acknowledge funding from NSF AGS-  
493 1822664. EAM acknowledges funding from NERC/EPSRC (award number EP/R513465/1). The  
494 authors acknowledge the Electric Power Research Institute (EPRI) and Southern Company for  
495 support of the SEARCH network and Atmospheric Research & Analysis. IMPROVE and CSN  
496 data are accessed from the Federal Land Manger Environmental Database. YZ thanks helpful  
497 discussions with Arlene M. Fiore, Róisín Commane and V. Faye McNeill.

498

### 499 **Author Contributions:**

500 Y.Z. and J.M. designed the research, performed the simulations and conducted the analysis.  
501 J.A.T. and E.M.M. provided guidance on aerosol coating parameterization. H.C. and D.K.H.  
502 provided the CrIS-derived NH<sub>3</sub> emission. N.L.N, W.H. and J.L.J. provided data from the  
503 SOAS2013 field campaign. E.E. provided data from the SEARCH network. Y.Z. wrote the paper  
with all coauthors providing input.

504

### 505 **Competing interests**

506 The authors declare no competing interests.

507

### 508 **Additional information**

509 Correspondence and material requests should be addressed to Y. Zheng and J. Mao.

510



- 511      **Reference:**
- 512      Ambro, E. L., Schobesberger, S., Gaston, C. J., Lopez-Hilfiker, F. D., Lee, B. H., Liu, J.,  
513      Zelenyuk, A., Bell, D., Cappa, C. D., Helgestad, T., Li, Z., Guenther, A., Wang, J., Wise, M.,  
514      Taylor, R., Surratt, J. D., Riedel, T., Hyttinen, N., Salo, V.-T., Hasan, G., Kurtén, T., Shilling, J.  
515      E. and Thornton, J. A.: Chamber-based insights into the factors controlling IEPOX SOA yield,  
516      composition, and volatility, *Atmos. Chem. Phys.*, 19, 11253–11265, doi:10.5194/acp-2019-271,  
517      2019.
- 518      Anttila, T., Kiendler-Scharr, A., Tillmann, R. and Mentel, T. F.: On the reactive uptake of  
519      gaseous compounds by organic-coated aqueous aerosols: Theoretical analysis and application to  
520      the heterogeneous hydrolysis of N<sub>2</sub>O<sub>5</sub>, *J. Phys. Chem. A*, 110(35), 10435–10443,  
521      doi:10.1021/jp062403c, 2006.
- 522      Attwood, A. R., Washenfelder, R. A., Brock, C. A., Hu, W., Baumann, K., Campuzano-Jost, P.,  
523      Day, D. A., Edgerton, E. S., Murphy, D. M., Palm, B. B., McComiskey, A., Wagner, N. L., De  
524      Sá, S. S., Ortega, A., Martin, S. T., Jimenez, J. L. and Brown, S. S.: Trends in sulfate and organic  
525      aerosol mass in the Southeast U.S.: Impact on aerosol optical depth and radiative forcing,  
526      *Geophys. Res. Lett.*, 41, 7701–7709, doi:10.1002/2014GL061669, 2014.
- 527      Bey, I., Jacob, D. J., Yantosca, R. M., Logan, J. A., Field, B. D., Fiore, A. M., Li, Q.-B., Liu, H.-  
528      Y., Mickley, L. J. and Schultz, M. G.: Global Modeling of Tropospheric Chemistry with  
529      Assimilated Meteorology: Model Description and Evaluation, *J. Geophys. Res.*, 106, 73–95,  
530      doi:10.1029/2001JD000807, 2001.
- 531      Bianchi, F., Kurtén, T., Riva, M., Mohr, C., Rissanen, M. P., Roldin, P., Berndt, T., Crounse, J.  
532      D., Wennberg, P. O., Mentel, T. F., Wildt, J., Junninen, H., Jokinen, T., Kulmala, M., Worsnop,  
533      D. R., Thornton, J. A., Donahue, N., Kjaergaard, H. G. and Ehn, M.: Highly Oxygenated Organic  
534      Molecules (HOM) from Gas-Phase Autoxidation Involving Peroxy Radicals: A Key Contributor  
535      to Atmospheric Aerosol, *Chem. Rev.*, 119(6), 3472–3509, doi:10.1021/acs.chemrev.8b00395,  
536      2019.
- 537      Blanchard, C. L., Hidy, G. M., Shaw, S., Baumann, K. and Edgerton, E. S.: Effects of emission  
538      reductions on organic aerosol in the southeastern United States, *Atmos. Chem. Phys.*, 16, 215–  
539      238, doi:10.5194/acp-16-215-2016, 2016.
- 540      Budisulistiorini, S. H., Li, X., Bairai, S. T., Renfro, J., Liu, Y., Liu, Y. J., McKinney, K. A.,  
541      Martin, S. T., McNeill, V. F., Pye, H. O. T., Nenes, A., Neff, M. E., Stone, E. A., Mueller, S.,  
542      Knote, C., Shaw, S. L., Zhang, Z., Gold, A. and Surratt, J. D.: Examining the effects of  
543      anthropogenic emissions on isoprene-derived secondary organic aerosol formation during the  
544      2013 Southern Oxidant and Aerosol Study (SOAS) at the Look Rock, Tennessee ground site,  
545      *Atmos. Chem. Phys.*, 15(15), 8871–8888, doi:10.5194/acp-15-8871-2015, 2015.
- 546      Budisulistiorini, S. H., Nenes, A., Carlton, A. G., Surratt, J. D., McNeill, V. F. and Pye, H. O. T.:  
547      Simulating Aqueous-Phase Isoprene-Epoxydiol (IEPOX) Secondary Organic Aerosol Production  
548      during the 2013 Southern Oxidant and Aerosol Study (SOAS), *Environ. Sci. Technol.*, 51(9),  
549      5026–5034, doi:10.1021/acs.est.6b05750, 2017.
- 550      Butler, T., Vermeylen, F., Lehmann, C. M., Likens, G. E. and Puchalski, M.: Increasing  
551      ammonia concentration trends in large regions of the USA derived from the NADP/AMoN  
552      network, *Atmos. Environ.*, 146(3), 132–140, doi:10.1016/j.atmosenv.2016.06.033, 2016.
- 553      Carlton, A. G., Pinder, R. W., Bhave, P. V. and Pouliot, G. A.: To what extent can biogenic SOA  
554      be controlled?, *Environ. Sci. Technol.*, 44(9), 3376–3380, doi:10.1021/es903506b, 2010.
- 555      Dammers, E., McLinden, C. A., Griffin, D., Shephard, M. W., Van Der Graaf, S., Lutsch, E.,  
556      Schaap, M., Gainairu-Matz, Y., Fioletov, V., Van Damme, M., Whitburn, S., Clarisse, L., Cady-



- 557 Pereira, K., Clerbaux, C., Francois Coheur, P. and Erisman, J. W.: NH<sub>3</sub> emissions from large  
558 point sources derived from CrIS and IASI satellite observations, *Atmos. Chem. Phys.*, 19(19),  
559 12261–12293, doi:10.5194/acp-19-12261-2019, 2019.  
560 Donahue, N. M., Robinson, a. L., Stanier, C. O. and Pandis, S. N.: Coupled partitioning,  
561 dilution, and chemical aging of semivolatile organics, *Environ. Sci. Technol.*, 40(8), 2635–2643,  
562 doi:10.1021/es052297c, 2006.  
563 Eddingsaas, N. C., Vandervelde, D. G. and Wennberg, P. O.: Kinetics and products of the acid-  
564 catalyzed ring-opening of atmospherically relevant butyl epoxy alcohols, *J. Phys. Chem. A*, 114,  
565 8106–8113, doi:10.1021/jp103907c, 2010.  
566 Edgerton, E. S., Hartsell, B. E., Saylor, R. D., Jansen, J. J., Hansen, D. A. and Hidy, G. M.: The  
567 southeastern aerosol research and characterization study: Part II. Filter-based measurements of  
568 fine and coarse particulate matter mass and composition, *J. Air Waste Manag. Assoc.*, 55(10),  
569 1527–1542, doi:10.1080/10473289.2005.10464744, 2005.  
570 EPA: The benefits and costs of the clean air act from 1990-2020, in *Better Air: Benefits and*  
571 *Costs of the Clean Air Act.*, 2011.  
572 Ervens, B., Turpin, B. J. and Weber, R. J.: Secondary organic aerosol formation in cloud droplets  
573 and aqueous particles (aqSOA): A review of laboratory, field and model studies, *Atmos. Chem.*  
574 *Phys.*, 11(21), 11069–11102, doi:10.5194/acp-11-11069-2011, 2011.  
575 Fisher, J. A., Jacob, D. J., Travis, K. R., Kim, P. S., Marais, E. A., Miller, C. C., Yu, K., Zhu, L.,  
576 Yantosca, R. M., Sulprizio, M. P., Mao, J., Wennberg, P. O., Crounse, J. D., Teng, A. P.,  
577 Nguyen, T. B., Clair, J. M. S., Cohen, R. C., Romer, P., Nault, B. A., Wooldridge, P. J., Jimenez,  
578 J. L., Campuzano-Jost, P., Day, D. A., Hu, W., Shepson, P. B., Xiong, F., Blake, D. R.,  
579 Goldstein, A. H., Misztal, P. K., Hanisco, T. F., Wolfe, G. M., Ryerson, T. B., Wisthaler, A. and  
580 Mikoviny, T.: Organic nitrate chemistry and its implications for nitrogen budgets in an isoprene-  
581 and monoterpane-rich atmosphere: Constraints from aircraft (SEAC4RS) and ground-based  
582 (SOAS) observations in the Southeast US, *Atmos. Chem. Phys.*, 16(9), 5969–5991,  
583 doi:10.5194/acp-16-5969-2016, 2016.  
584 Fountoukis, C. and Nenes, A.: ISORROPIA II: a computationally efficient thermodynamic  
585 equilibrium model for K<sup>+</sup>-Ca<sup>2+</sup>-Mg<sup>2+</sup>-NH<sub>4</sub><sup>+</sup>-Na<sup>+</sup>-SO<sub>4</sub><sup>2-</sup>-NO<sub>3</sub><sup>-</sup>-Cl<sup>-</sup>-H<sub>2</sub>O aerosols, *Atmos.*  
586 *Chem. Phys.*, 7, 4639–4659, doi:10.5194/acp-7-4639-2007, 2007.  
587 Fu, T. M., Jacob, D. J., Wittrock, F., Burrows, J. P., Vrekoussis, M. and Henze, D. K.: Global  
588 budgets of atmospheric glyoxal and methylglyoxal, and implications for formation of secondary  
589 organic aerosols, *J. Geophys. Res. Atmos.*, doi:10.1029/2007JD009505, 2008.  
590 Gaston, C. J., Riedel, T. P., Zhang, Z., Gold, A., Surratt, J. D. and Thornton, J. A.: Reactive  
591 uptake of an isoprene-derived epoxydiol to submicron aerosol particles, *Environ. Sci. Technol.*,  
592 48(19), 11178–11186, doi:10.1021/es5034266, 2014.  
593 Guenther, A. B., Karl, T., Harley, P., Wiedinmyer, C., Palmer, P. I. and Geron, C.: Estimates of  
594 global terrestrial isoprene emissions using MEGAN (Model of Emissions of Gases and Aerosols  
595 from Nature), *Atmos. Chem. Phys.*, 6, 3181–3210, doi:doi:10.5194/acp-6-3181-2006, 2006.  
596 Guenther, A. B., Jiang, X., Heald, C. L., Sakulyanontvittaya, T., Duhl, T., Emmons, L. K. and  
597 Wang, X.: The model of emissions of gases and aerosols from nature version 2.1 (MEGAN2.1):  
598 An extended and updated framework for modeling biogenic emissions, *Geosci. Model Dev.*, 5,  
599 1471–1492, doi:10.5194/gmd-5-1471-2012, 2012.  
600 Guo, H., Xu, L., Bougiatioti, A., Cerully, K. M., Capps, S. L., Hite, J. R., Carlton, A. G., Lee, S.  
601 H., Bergin, M. H., Ng, N. L., Nenes, A. and Weber, R. J.: Fine-particle water and pH in the  
602 southeastern United States, *Atmos. Chem. Phys.*, 15(9), 5211–5228, doi:10.5194/acp-15-5211-



- 603 2015, 2015.  
604 Guo, H., Nenes, A. and Weber, R. J.: The underappreciated role of nonvolatile cations in aerosol  
605 ammonium-sulfate molar ratios, *Atmos. Chem. Phys.*, 18(23), 17307–17323, doi:10.5194/acp-  
606 18-17307-2018, 2018.  
607 Hayes, P. L., Carlton, A. G., Baker, K. R., Ahmadov, R., Washenfelder, R. A., Alvarez, S.,  
608 Rappenglück, B., Gilman, J. B., Kuster, W. C., De Gouw, J. A., Zotter, P., Prévôt, A. S. H.,  
609 Szidat, S., Kleindienst, T. E., Offenberg, J. H., Ma, P. K. and Jimenez, J. L.: Modeling the  
610 formation and aging of secondary organic aerosols in Los Angeles during CalNex 2010, *Atmos.*  
611 *Chem. Phys.*, 15(10), 5773–5801, doi:10.5194/acp-15-5773-2015, 2015.  
612 Henze, D. K., Hakami, A. and Seinfeld, J. H.: Development of the adjoint of GEOS-Chem,  
613 *Atmos. Chem. Phys.*, 7(9), 2413–2433, doi:10.5194/acp-7-2413-2007, 2007.  
614 Hidy, G. M., Blanchard, C. L., Baumann, K., Edgerton, E., Tanenbaum, S., Shaw, S., Knipping,  
615 E., Tombach, I., Jansen, J. and Walters, J.: Chemical climatology of the southeastern United  
616 States, 1999–2013, *Atmos. Chem. Phys.*, 14(21), 11893–11914, doi:10.5194/acp-14-11893-2014,  
617 2014.  
618 Hodshire, A. L., Akherati, A., Alvarado, M. J., Brown-Steiner, B., Jathar, S. H., Jimenez, J. L.,  
619 Kreidenweis, S. M., Lonsdale, C. R., Onasch, T. B., Ortega, A. M. and Pierce, J. R.: Aging  
620 Effects on Biomass Burning Aerosol Mass and Composition: A Critical Review of Field and  
621 Laboratory Studies, *Environ. Sci. Technol.*, 53(17), 10007–10022, doi:10.1021/acs.est.9b02588,  
622 2019.  
623 Hu, W., Palm, B. B., Day, D. A., Campuzano-Jost, P., Krechmer, J. E., Peng, Z., De Sa Suzane,  
624 S., Martin, S. T., Alexander, M. L., Baumann, K., Hacker, L., Kiendler-Scharr, A., Koss, A. R.,  
625 De Gouw, J. A., Goldstein, A. H., Seco, R., Sjostedt, S. J., Park, J. H., Guenther, A. B., Kim, S.,  
626 Canonaco, F., Prévôt, A. S. H., Brune, W. H. and Jimenez, J. L.: Volatility and lifetime against  
627 OH heterogeneous reaction of ambient isoprene-epoxydiols-derived secondary organic aerosol  
628 (IEPOX-SOA), *Atmos. Chem. Phys.*, 16(18), 11563–11580, doi:10.5194/acp-16-11563-2016,  
629 2016.  
630 Hu, W. W., Campuzano-Jost, P., Palm, B. B., Day, D. A., Ortega, A. M., Hayes, P. L.,  
631 Krechmer, J. E., Chen, Q., Kuwata, M., Liu, Y. J., De Sá, S. S., McKinney, K., Martin, S. T., Hu,  
632 M., Budisulistiorini, S. H., Riva, M., Surratt, J. D., St. Clair, J. M., Isaacman-Van Wertz, G.,  
633 Yee, L. D., Goldstein, A. H., Carbone, S., Brito, J., Artaxo, P., De Gouw, J. A., Koss, A.,  
634 Wisthaler, A., Mikoviny, T., Karl, T., Kaser, L., Jud, W., Hansel, A., Docherty, K. S., Alexander,  
635 M. L., Robinson, N. H., Coe, H., Allan, J. D., Canagaratna, M. R., Paulot, F. and Jimenez, J. L.:  
636 Characterization of a real-time tracer for isoprene epoxydiols-derived secondary organic aerosol  
637 (IEPOX-SOA) from aerosol mass spectrometer measurements, *Atmos. Chem. Phys.*, 15(20),  
638 11807–11833, doi:10.5194/acp-15-11807-2015, 2015.  
639 Isaacman-VanWertz, G., Yee, L. D., Kreisberg, N. M., Wernis, R., Moss, J. A., Hering, S. V., De  
640 Sá, S. S., Martin, S. T., Alexander, M. L., Palm, B. B., Hu, W., Campuzano-Jost, P., Day, D. A.,  
641 Jimenez, J. L., Riva, M., Surratt, J. D., Viegas, J., Manzi, A., Edgerton, E., Baumann, K., Souza,  
642 R., Artaxo, P. and Goldstein, A. H.: Ambient Gas-Particle Partitioning of Tracers for Biogenic  
643 Oxidation, *Environ. Sci. Technol.*, 50(18), 9952–9962, doi:10.1021/acs.est.6b01674, 2016.  
644 Janssens-Maenhout, G., Crippa, M., Guizzardi, D., Dentener, F., Muntean, M., Pouliot, G.,  
645 Keating, T., Zhang, Q., Kurokawa, J., Wankmüller, R., Denier Van Der Gon, H., Kuenen, J. J.  
646 P., Klimont, Z., Frost, G., Darras, S., Koffi, B. and Li, M.: HTAP-v2.2: A mosaic of regional and  
647 global emission grid maps for 2008 and 2010 to study hemispheric transport of air pollution,  
648 *Atmos. Chem. Phys.*, 15(19), 11411–11432, doi:10.5194/acp-15-11411-2015, 2015.



- 649 Jimenez, J. L., Canagaratna, M. R., Donahue, N. M., Prevot, A. S. H., Zhang, Q., Kroll, J. H.,  
650 DeCarlo, P. F., Allan, J. D., Coe, H., Ng, N. L., Aiken, A. C., Docherty, K. S., Ulbrich, I. M.,  
651 Grieshop, A. P., Robinson, A. L., Duplissy, J., Smith, J. D., Wilson, K. R., Lanz, V. A., Hueglin,  
652 C., Sun, Y. L., Tian, J., Laaksonen, A., Raatikainen, T., Rautiainen, J., Vaattovaara, P., Ehn, M.,  
653 Kulmala, M., Tomlinson, J. M., Collins, D. R., Cubison, M. J., Dunlea, E. J., Huffman, J. A.,  
654 Onasch, T. B., Alfarra, M. R., Williams, P. I., Bower, K., Kondo, Y., Schneider, J., Drewnick, F.,  
655 Borrmann, S., Weimer, S., Demerjian, K., Salcedo, D., Cottrell, L., Griffin, R., Takami, A.,  
656 Miyoshi, T., Hatakeyama, S., Shimono, A., Sun, J. Y., Zhang, Y. M., Dzepina, K., Kimmel, J.  
657 R., Sueper, D., Jayne, J. T., Herndon, S. C., Trimborn, A. M., Williams, L. R., Wood, E. C.,  
658 Middlebrook, A. M., Kolb, C. E., Baltensperger, U. and Worsnop, D. R.: Evolution of organic  
659 aerosols in the atmosphere, *Science* (80-.), 326(5959), 1525–1529,  
660 doi:10.1126/science.1180353, 2009.  
661 Jo, D. S., Hodzic, A., Emmons, L. K., Marais, E. A., Peng, Z., Nault, B. A., Hu, W.,  
662 Campuzano-Jost, P. and Jimenez, J. L.: A simplified parameterization of isoprene-epoxydiol-  
663 derived secondary organic aerosol (IEPOX-SOA) for global chemistry and climate models: A  
664 case study with GEOS-Chem v11-02-rc, *Geosci. Model Dev.*, 12(7), 2983–3000,  
665 doi:10.5194/gmd-12-2983-2019, 2019.  
666 Kiendler-Scharr, A., Mensah, A. A., Friese, E., Topping, D., Nemitz, E., Prevot, A. S. H., Äijälä,  
667 M., Allan, J., Canonaco, F., Canagaratna, M., Carbone, S., Crippa, M., Dall Osto, M., Day, D.  
668 A., De Carlo, P., Di Marco, C. F., Elbern, H., Eriksson, A., Freney, E., Hao, L., Herrmann, H.,  
669 Hildebrandt, L., Hillamo, R., Jimenez, J. L., Laaksonen, A., McFiggans, G., Mohr, C., O'Dowd,  
670 C., Otjes, R., Ovadnevaite, J., Pandis, S. N., Poulain, L., Schlag, P., Sellegrí, K., Swietlicki, E.,  
671 Tiitta, P., Vermeulen, A., Wahner, A., Worsnop, D. and Wu, H. C.: Ubiquity of organic nitrates  
672 from nighttime chemistry in the European submicron aerosol, *Geophys. Res. Lett.*, 43(14), 7735–  
673 7744, doi:10.1002/2016GL069239, 2016.  
674 Kim, P. S., Jacob, D. J., Fisher, J. A., Travis, K., Yu, K., Zhu, L., Yantosca, R. M., Sulprizio, M.  
675 P., Jimenez, J. L., Campuzano-Jost, P., Froyd, K. D., Liao, J., Hair, J. W., Fenn, M. A., Butler, C.  
676 F., Wagner, N. L., Gordon, T. D., Welti, A., Wennberg, P. O., Crounse, J. D., St. Clair, J. M.,  
677 Teng, A. P., Millet, D. B., Schwarz, J. P., Markovic, M. Z. and Perring, A. E.: Sources,  
678 seasonality, and trends of Southeast US aerosol: An integrated analysis of surface, aircraft, and  
679 satellite observations with the GEOS-Chem chemical transport model, *Atmos. Chem. Phys.*  
680 *Discuss.*, 15(13), 17651–17709, doi:10.5194/acpd-15-17651-2015, 2015.  
681 Kroll, J. H., Ng, N. L., Murphy, S. M., Flagan, R. C. and Seinfeld, J. H.: Secondary organic  
682 aerosol formation from isoprene photooxidation under high-NO<sub>x</sub> conditions, *Geophys. Res.*  
683 *Lett.*, 32(x), 1–4, doi:10.1029/2005GL023637, 2005.  
684 Kroll, J. H., Ng, N. L., Murphy, S. M., Flagan, R. C. and Seinfeld, J. H.: Secondary organic  
685 aerosol formation from isoprene photooxidation, *Environ. Sci. Technol.*, 40(3), 1869–1877,  
686 doi:10.1021/es0524301, 2006.  
687 Li, J., Mao, J., Min, K. E., Washenfelder, R. A., Brown, S. S., Kaiser, J., Keutsch, F. N.,  
688 Volkamer, R., Wolfe, G. M., Hanisco, T. F., Pollack, I. B., Ryerson, T. B., Graus, M., Gilman, J.  
689 B., Lerner, B. M., Warneke, C., de Gouw, J. A., Middlebrook, A. M., Liao, J., Welti, A.,  
690 Henderson, B. H., Faye McNeill, V., Hall, S. R., Ullmann, K., Donner, L. J., Paulot, F. and  
691 Horowitz, L. W.: Observational constraints on glyoxal production from isoprene oxidation and  
692 its contribution to organic aerosol over the Southeast United States, *J. Geophys. Res.*,  
693 doi:10.1002/2016JD025331, 2016.  
694 Li, J., Mao, J., Fiore, A. M., Cohen, R. C., Crounse, J. D., Teng, A. P., Wennberg, P. O., Lee, B.



- 695 H., Lopez-Hilfiker, F. D., Thornton, J. A., Peischl, J., Pollack, I. B., Ryerson, T. B., Veres, P.,  
696 Roberts, J. M., Neuman, J. A., Nowak, J. B., Wolfe, G. M., Hanisco, T. F., Fried, A., Singh, H.  
697 B., Dibb, J., Paulot, F. and Horowitz, L. W.: Decadal changes in summertime reactive oxidized  
698 nitrogen and surface ozone over the Southeast United States, *Atmos. Chem. Phys.*, 18(3), 2341–  
699 2361, doi:10.5194/acp-18-2341-2018, 2018.
- 700 Liggio, J., Li, S. M. and McLaren, R.: Reactive uptake of glyoxal by particulate matter, *J.  
701 Geophys. Res. D Atmos.*, 110(10), 1–13, doi:10.1029/2004JD005113, 2005.
- 702 Lin, Y. H., Knipping, E. M., Edgerton, E. S., Shaw, S. L. and Surratt, J. D.: Investigating the  
703 influences of SO<sub>2</sub> and NH<sub>3</sub> levels on isoprene-derived secondary organic aerosol formation  
704 using conditional sampling approaches, *Atmos. Chem. Phys.*, 13(16), 8457–8470,  
705 doi:10.5194/acp-13-8457-2013, 2013.
- 706 Lopez-Hilfiker, F. D., Mohr, C., D'Ambro, E. L., Lutz, A., Riedel, T. P., Gaston, C. J., Iyer, S.,  
707 Zhang, Z., Gold, A., Surratt, J. D., Lee, B. H., Kurten, T., Hu, W. W., Jimenez, J., Hallquist, M.  
708 and Thornton, J. A.: Molecular Composition and Volatility of Organic Aerosol in the  
709 Southeastern U.S.: Implications for IEPOX Derived SOA, *Environ. Sci. Technol.*, 50(5), 2200–  
710 2209, doi:10.1021/acs.est.5b04769, 2016.
- 711 Malm, W. C., Schichtel, B. A., Hand, J. L. and Collett, J. L.: Concurrent Temporal and Spatial  
712 Trends in Sulfate and Organic Mass Concentrations Measured in the IMPROVE Monitoring  
713 Program, *J. Geophys. Res. Atmos.*, 122(19), 10462–10476, doi:10.1002/2017JD026865, 2017.
- 714 Mao, J., Paulot, F., Jacob, D. J., Cohen, R. C., Crounse, J. D., Wennberg, P. O., Keller, C. A.,  
715 Hudman, R. C., Barkley, M. P. and Horowitz, L. W.: Ozone and organic nitrates over the eastern  
716 United States: Sensitivity to isoprene chemistry, *J. Geophys. Res. Atmos.*, 118(19), 11256–  
717 11268, doi:10.1002/jgrd.50817, 2013.
- 718 Mao, J., Carlton, A., Cohen, R. C., Brune, W. H., Brown, S. S., Wolfe, G. M., Jimenez, J. L.,  
719 Pye, H. O. T., Lee Ng, N., Xu, L., Faye McNeill, V., Tsigaridis, K., McDonald, B. C., Warneke,  
720 C., Guenther, A., Alvarado, M. J., De Gouw, J., Mickley, L. J., Leibensperger, E. M., Mathur,  
721 R., Nolte, C. G., Portmann, R. W., Unger, N., Tosca, M. and Horowitz, L. W.: Southeast  
722 Atmosphere Studies: Learning from model-observation syntheses, *Atmos. Chem. Phys.*, 18(4),  
723 2615–2651, doi:10.5194/acp-18-2615-2018, 2018.
- 724 Marais, E. A., Jacob, D. J., Jimenez, J. L., Campuzano-Jost, P., Day, D. A., Hu, W., Krechmer,  
725 J., Zhu, L., Kim, P. S., Miller, C. C., Fisher, J. A., Travis, K., Yu, K., Hanisco, T. F., Wolfe, G.  
726 M., Arkinson, H. L., Pye, H. O. T., Froyd, K. D., Liao, J. and McNeill, V. F.: Aqueous-phase  
727 mechanism for secondary organic aerosol formation from isoprene: Application to the Southeast  
728 United States and co-benefit of SO<sub>2</sub> emission controls, *Atmos. Chem. Phys.*, 16, 1603–1618,  
729 doi:10.5194/acp-16-1603-2016, 2016.
- 730 Marais, E. A., Jacob, D. J., Turner, J. R. and Mickley, L. J.: Evidence of 1991–2013 decrease of  
731 biogenic secondary organic aerosol in response to SO<sub>2</sub> emission controls, *Environ. Sci.  
732 Technol.*, 12, doi:<https://doi.org/10.1088/1748-9326/aa69c8>, 2017.
- 733 McNeill, V. F., Woo, J. L., Kim, D. D., Schwier, A. N., Wannell, N. J., Sumner, A. J. and  
734 Barakat, J. M.: Aqueous-phase secondary organic aerosol and organosulfate formation in  
735 atmospheric aerosols: A modeling study, *Environ. Sci. Technol.*, 46(15), 8075–8081,  
736 doi:10.1021/es3002986, 2012.
- 737 Murphy, D. M., Cziczo, D. J., Froyd, K. D., Hudson, P. K., Matthew, B. M., Middlebrook, A.  
738 M., Peltier, R. E., Sullivan, A., Thomson, D. S. and Weber, R. J.: Single-peptide mass  
739 spectrometry of tropospheric aerosol particles, *J. Geophys. Res. Atmos.*, 111(23), 1–15,  
740 doi:10.1029/2006JD007340, 2006.



- 741 Ng, N. L., Brown, S. S., Archibald, A. T., Atlas, E., Cohen, R. C., Crowley, J. N., Day, D. A.,  
742 Donahue, N. M., Fry, J. L., Fuchs, H., Griffin, R. J., Guzman, M. I., Herrmann, H., Hodzic, A.,  
743 Iinuma, Y., Kiendler-Scharr, A., Lee, B. H., Luecken, D. J., Mao, J., McLaren, R., Mutzel, A.,  
744 Osthoff, H. D., Ouyang, B., Picquet-Varrault, B., Platt, U., Pye, H. O. T., Rudich, Y., Schwantes,  
745 R. H., Shiraiwa, M., Stutz, J., Thornton, J. A., Tilgner, A., Williams, B. J. and Zaveri, R. A.:  
746 Nitrate radicals and biogenic volatile organic compounds: Oxidation, mechanisms, and organic  
747 aerosol, *Atmos. Chem. Phys.*, 17(3), 2103–2162, doi:10.5194/acp-17-2103-2017, 2017.  
748 Nguyen, T. B., Coggon, M. M., Bates, K. H., Zhang, X., Schwantes, R. H., Schilling, K. A.,  
749 Loza, C. L., Flagan, R. C., Wennberg, P. O. and Seinfeld, J. H.: Organic aerosol formation from  
750 the reactive uptake of isoprene epoxydiols (IEPOX) onto non-acidified inorganic seeds, *Atmos.*  
751 *Chem. Phys.*, 14(7), 3497–3510, doi:10.5194/acp-14-3497-2014, 2014.  
752 Pankow, J. F.: An Absorption-Model of the Gas Aerosol Partitioning Involved in the Formation  
753 of Secondary Organic Aerosol, *Atmos. Environ.*, 28(2), 189–193,  
754 doi:10.1016/j.atmosenv.2007.10.060, 1994.  
755 Paulot, F., Crounse, J. D., Kjaergaard, H. G., Kürten, A., Clair, J. M. S., Seinfeld, J. H. and  
756 Wennberg, P. O.: Unexpected Epoxide Formation in the Gas-Phase Photooxidation of Isoprene,  
757 *Science* (80- ), 325, 730–734, doi:10.1126/science.1174251, 2009.  
758 Paulot, F., Jacob, D. J., Pinder, R. W., Bash, J. O., Travis, K. R. and Henze, D. K.: Ammonia  
759 emissions in the United States, European Union, and China derived by high-resolution inversion  
760 of ammonium wet deposition data: Interpretation with a new agricultural emissions inventory  
761 (MASAGE\_NH3), *J. Geophys. Res. Atmos.*, 119, 4343–4364, doi:doi:10.1002/2013JD021130,  
762 2014.  
763 Presto, A. a., Huff Hartz, K. E. and Donahue, N. M.: Secondary organic aerosol production from  
764 terpene ozonolysis. 2. Effect of NO<sub>x</sub> concentration, *Environ. Sci. Technol.*, 39(18), 7046–7054,  
765 doi:10.1021/es050400s, 2005.  
766 Pye, H. O. T., Liao, H., Wu, S., Mickley, L. J., Jacob, D. J., Henze, D. J. and Seinfeld, J. H.:  
767 Effect of changes in climate and emissions on future sulfate-nitrate-ammonium aerosol levels in  
768 the United States, *J. Geophys. Res. Atmos.*, 114(1), 1–18, doi:10.1029/2008JD010701, 2009.  
769 Pye, H. O. T., Chan, a. W. H., Barkley, M. P. and Seinfeld, J. H.: Global modeling of organic  
770 aerosol: The importance of reactive nitrogen (NO<sub>x</sub> and NO<sub>3</sub>), *Atmos. Chem. Phys.*, 10, 11261–  
771 11276, doi:10.5194/acp-10-11261-2010, 2010.  
772 Pye, H. O. T., Pinder, R. W., Piletic, I. R., Xie, Y., Capps, S. L., Lin, Y. H., Surratt, J. D., Zhang,  
773 Z., Gold, A., Luecken, D. J., Hutzell, W. T., Jaoui, M., Offenberg, J. H., Kleindienst, T. E.,  
774 Lewandowski, M. and Edney, E. O.: Epoxide pathways improve model predictions of isoprene  
775 markers and reveal key role of acidity in aerosol formation, *Environ. Sci. Technol.*, 47(19),  
776 11056–11064, doi:10.1021/es402106h, 2013.  
777 Pye, H. O. T., Murphy, B. N., Xu, L., Ng, N. L., Carlton, A. G., Guo, H., Weber, R., Vasilakos,  
778 P., Wyat Appel, K., Hapsari Budisulistiorini, S., Surratt, J. D., Nenes, A., Hu, W., Jimenez, J. L.,  
779 Isaacman-Vanwertz, G., Misztal, P. K. and Goldstein, A. H.: On the implications of aerosol  
780 liquid water and phase separation for organic aerosol mass, *Atmos. Chem. Phys.*, 17(1), 343–  
781 369, doi:10.5194/acp-17-343-2017, 2017.  
782 Pye, H. O. T., D'Ambro, E. L., Lee, B. H., Schobesberger, S., Takeuchi, M., Zhao, Y., Lopez-  
783 Hilfiker, F., Liu, J., Shilling, J. E., Xing, J., Mathur, R., Middlebrook, A. M., Liao, J., Welti, A.,  
784 Graus, M., Warneke, C., de Gouw, J. A., Holloway, J. S., Ryerson, T. B., Pollack, I. B. and  
785 Thornton, J. A.: Anthropogenic enhancements to production of highly oxygenated molecules  
786 from autoxidation, *Proc. Natl. Acad. Sci. U. S. A.*, 116(14), 6641–6646,



- 787 doi:10.1073/pnas.1810774116, 2019a.  
788 Pye, H. O. T., Nenes, A., Alexander, B., Ault, A. P., Barth, M. C., Simon, L., Collett, J. L.,  
789 Fahey, K. M., Hennigan, C. J., Herrmann, H., Kanakidou, M., Kelly, J. T., Ku, I., Mcneill, V. F.,  
790 Riemer, N., Shi, G., Tilgner, A., Walker, J. T., Wang, T., Weber, R., Xing, J., Zaveri, R. A. and  
791 Zuend, A.: The Acidity of Atmospheric Particles and Clouds, *Atmos. Chem. Phys. Atmos. Chem. Phys.*, (October), 2019b.  
792 Randerson, J. T., van der Werf, G. R., Giglio, L., Collatz, G. J. and Kasibhatla, P. S.: Global Fire  
793 Emissions Database, Version 4, (GFEDv4), ORNL DAAC, doi:10.3334/ORNLDAAAC/1293,  
794 2015.  
795 Ridley, D. A., Heald, C. L., Ridley, K. J. and Kroll, J. H.: Causes and consequences of  
796 decreasing atmospheric organic aerosol in the United States, *Proc. Natl. Acad. Sci. U. S. A.*,  
797 115(2), 290–295, doi:10.1073/pnas.1700387115, 2018.  
798 Riedel, T. P., Lin, Y. H., Budisulistiorini, S. H., Gaston, C. J., Thornton, J. A., Zhang, Z.,  
799 Vizuete, W., Gold, A. and Surratt, J. D.: Heterogeneous reactions of isoprene-derived epoxides:  
800 Reaction probabilities and molar secondary organic aerosol yield estimates, *Environ. Sci. Technol. Lett.*, 2(2), 38–42, doi:10.1021/ez500406f, 2015.  
801 Riedel, T. P., Lin, Y. H., Zhang, Z., Chu, K., Thornton, J. A., Vizuete, W., Gold, A. and Surratt,  
802 J. D.: Constraining condensed-phase formation kinetics of secondary organic aerosol  
803 components from isoprene epoxydiols, *Atmos. Chem. Phys.*, 16(3), 1245–1254,  
804 doi:10.5194/acp-16-1245-2016, 2016.  
805 Riva, M., Bell, D. M., Hansen, A. M. K., Drozd, G. T., Zhang, Z., Gold, A., Imre, D., Surratt, J.  
806 D., Glasius, M. and Zelenyuk, A.: Effect of Organic Coatings, Humidity and Aerosol Acidity on  
807 Multiphase Chemistry of Isoprene Epoxydiols, *Environ. Sci. Technol.*, 50(11), 5580–5588,  
808 doi:10.1021/acs.est.5b06050, 2016.  
809 Riva, M., Chen, Y., Zhang, Y., Lei, Z., Olson, N. E., Boyer, H. C., Narayan, S., Yee, L. D.,  
810 Green, H. S., Cui, T., Zhang, Z., Baumann, K., Fort, M., Edgerton, E., Budisulistiorini, S. H.,  
811 Rose, C. A., Ribeiro, I. O., e Oliveira, R. L., dos Santos, E. O., Machado, C. M. D., Szopa, S.,  
812 Zhao, Y., Alves, E. G., de Sá, S. S., Hu, W., Knipping, E. M., Shaw, S. L., Duvoisin Junior, S.,  
813 de Souza, R. A. F., Palm, B. B., Jimenez, J.-L., Glasius, M., Goldstein, A. H., Pye, H. O. T.,  
814 Gold, A., Turpin, B. J., Vizuete, W., Martin, S. T., Thornton, J. A., Dutcher, C. S., Ault, A. P.  
815 and Surratt, J. D.: Increasing Isoprene Epoxydiol-to-Inorganic Sulfate Aerosol Ratio Results in  
816 Extensive Conversion of Inorganic Sulfate to Organosulfur Forms: Implications for Aerosol  
817 Physicochemical Properties, *Environ. Sci. Technol.*, 53(15), 8682–8694,  
818 doi:10.1021/acs.est.9b01019, 2019.  
819 Schroder, J. C., Campuzano-Jost, P., Day, D. A., Shah, V., Larson, K., Sommers, J. M., Sullivan,  
820 A. P., Campos, T., Reeves, J. M., Hills, A., Hornbrook, R. S., Blake, N. J., Scheuer, E., Guo, H.,  
821 Fibiger, D. L., McDuffie, E. E., Hayes, P. L., Weber, R. J., Dibb, J. E., Apel, E. C., Jaeglé, L.,  
822 Brown, S. S., Thornton, J. A. and Jimenez, J. L.: Sources and Secondary Production of Organic  
823 Aerosols in the Northeastern United States during WINTER, *J. Geophys. Res. Atmos.*, 123(14),  
824 7771–7796, doi:10.1029/2018JD028475, 2018.  
825 Schwantes, R. H., Charan, S. M., Bates, K. H., Huang, Y., Nguyen, T. B., Mai, H., Kong, W.,  
826 Flagan, R. C. and Seinfeld, J. H.: Low-volatility compounds contribute significantly to isoprene  
827 secondary organic aerosol (SOA) under high-NO<sub>x</sub> conditions, *Atmos. Chem. Phys.*, 19(11),  
828 7255–7278, doi:10.5194/acp-19-7255-2019, 2019.  
829 Shah, V., Jaeglé, L., Jimenez, J. L., Schroder, J. C., Campuzano-Jost, P., Campos, T. L., Reeves,  
830 J. M., Stell, M., Brown, S. S., Lee, B. H., Lopez-Hilfiker, F. D. and Thornton, J. A.: Widespread



- 833 Pollution From Secondary Sources of Organic Aerosols During Winter in the Northeastern  
834 United States, *Geophys. Res. Lett.*, 46(5), 2974–2983, doi:10.1029/2018GL081530, 2019.  
835 Shephard, M. W. and Cady-Pereira, K. E.: Cross-track Infrared Sounder (CrIS) satellite  
836 observations of tropospheric ammonia, *Atmos. Meas. Tech.*, 8(3), 1323–1336, doi:10.5194/amt-  
837 8-1323-2015, 2015.  
838 Shrivastava, M., Cappa, C. D., Fan, J., Goldstein, A. H., Guenther, A. B., Jimenez, J. L., Kuang,  
839 Laskin, A., Martin, S. T., Ng, N. L., Petaja, T., Pierce, J. R., Rasch, P. J., Roldin, P., Seinfeld,  
840 J. H., Shilling, J., Smith, J. N., Thornton, J. A., Volkamer, R., Wang, J., Worsnop, D. R., Zaveri,  
841 R. A., Zelenyuk, A. and Zhang, Q.: Recent advances in understanding secondary organic aerosol:  
842 Implications for global climate forcing, *Rev. Geophys.*, 55(2), 509–559,  
843 doi:10.1002/2016RG000540, 2017.  
844 Shrivastava, M., Andreae, M. O., Artaxo, P., Barbosa, H. M. J., Berg, L. K., Brito, J., Ching, J.,  
845 Easter, R. C., Fan, J., Fast, J. D., Feng, Z., Fuentes, J. D., Glasius, M., Goldstein, A. H., Alves, E.  
846 Gomes, H., Gu, D., Guenther, A., Jathar, S. H., Kim, S., Liu, Y., Lou, S., Martin, S. T.,  
847 McNeill, V. F., Medeiros, A., de Sá, S. S., Shilling, J. E., Springston, S. R., Souza, R. A. F.,  
848 Thornton, J. A., Isaacman-VanWertz, G., Yee, L. D., Ynoue, R., Zaveri, R. A., Zelenyuk, A. and  
849 Zhao, C.: Urban pollution greatly enhances formation of natural aerosols over the Amazon  
850 rainforest, *Nat. Commun.*, 10(1), doi:10.1038/s41467-019-08909-4, 2019.  
851 Silvern, R. F., Jacob, D. J., Kim, P. S., Marais, E. A., Turner, J. R., Campuzano-Jost, P. and  
852 Jimenez, J. L.: Inconsistency of ammonium-sulfate aerosol ratios with thermodynamic models in  
853 the eastern US: A possible role of organic aerosol, *Atmos. Chem. Phys.*, 17(8), 5107–5118,  
854 doi:10.5194/acp-17-5107-2017, 2017.  
855 Solomon, P. A., Crumpler, D., Flanagan, J. B., Jayanty, R. K. M., Rickman, E. E. and McDade,  
856 C. E.: U.S. National PM2.5 chemical speciation monitoring networks—CSN and IMPROVE:  
857 Description of networks, *J. Air Waste Manag. Assoc.*, 64(12), 1410–1438,  
858 doi:10.1080/10962247.2014.956904, 2014.  
859 Song, S., Gao, M., Xu, W., Shao, J., Shi, G., Wang, S., Wang, Y., Sun, Y. and McElroy, M. B.:  
860 Fine-particle pH for Beijing winter haze as inferred from different thermodynamic equilibrium  
861 models, *Atmos. Chem. Phys.*, 18(10), 7423–7438, doi:10.5194/acp-18-7423-2018, 2018.  
862 Surratt, J. D., Lewandowski, M., Offenberg, J. H., Jaoui, M., Kleindienst, T. E., Edney, E. O. and  
863 Seinfeld, J. H.: Effect of acidity on secondary organic aerosol formation from isoprene, *Environ. Sci. Technol.*, (41), 5363–5369, doi:10.1021/es0704176, 2007a.  
864 Surratt, J. D., Kroll, J. H., Kleindienst, T. E., Edney, E. O., Claeys, M., Sorooshian, A., Ng, N.  
865 L., Offenberg, J. H., Lewandowski, M., Jaoui, M., Flagan, R. C. and Seinfeld, J. H.: Evidence for  
866 organosulfates in secondary organic aerosol, *Environ. Sci. Technol.*, (41), 517–527,  
867 doi:10.1021/es062081q, 2007b.  
868 Surratt, J. D., Chan, A. W. H., Eddingsaas, N. C., Chan, M., Loza, C. L., Kwan, A. J., Hersey, S.  
869 P., Flagan, R. C., Wennberg, P. O. and Seinfeld, J. H.: Reactive intermediates revealed in  
870 secondary organic aerosol formation from isoprene, *Proc. Natl. Acad. Sci.*, 107(15), 6640–6645,  
871 doi:10.1073/pnas.0911114107, 2010.  
872 Tan, Y., Lim, Y. B., Altieri, K. E., Seitzinger, S. P. and Turpin, B. J.: Mechanisms leading to  
873 oligomers and SOA through aqueous photooxidation: Insights from OH radical oxidation of  
874 acetic acid and methylglyoxal, *Atmos. Chem. Phys.*, 12(2), 801–813, doi:10.5194/acp-12-801-  
875 2012, 2012.  
876 Tao, Y. and Murphy, J. G.: The sensitivity of PM2.5 acidity to meteorological parameters and  
877 chemical composition changes: 10-year records from six Canadian monitoring sites, *Atmos.*  
878



- 879 Chem. Phys. Discuss., 1–21, doi:10.5194/acp-2019-238, 2019.  
880 Travis, K. R., Jacob, D. J., Fisher, J. A., Kim, P. S., Marais, E. A., Zhu, L., Yu, K., Miller, C. C.,  
881 Yantosca, R. M., Sulprizio, M. P., Thompson, A. M., Wennberg, P. O., Crounse, J. D., St Clair,  
882 J. M., Cohen, R. C., Laughner, J. L., Dibb, J. E., Hall, S. R., Ullmann, K., Wolfe, G. M., Pollack,  
883 I. B., Peischl, J., Neuman, J. A. and Zhou, X.: Why do models overestimate surface ozone in the  
884 Southeast United States?, Atmos. Chem. Phys., 16(21), 13561–13577, doi:10.5194/acp-16-  
885 13561-2016, 2016.  
886 Tsui, W. G., Woo, J. L. and Mcneill, V. F.: Impact of Aerosol-Cloud Cycling on Aqueous  
887 Secondary Organic Aerosol Formation, Atmosphere (Basel)., 10, 666,  
888 doi:doi:10.3390/atmos10110666, 2019.  
889 Wagner, N. L., Brock, C. A., Angevine, W. M., Beyersdorf, A., Campuzano-Jost, P., Day, D., De  
890 Gouw, J. A., Diskin, G. S., Gordon, T. D., Graus, M. G., Holloway, J. S., Huey, G., Jimenez, J.  
891 L., Lack, D. A., Liao, J., Liu, X., Markovic, M. Z., Middlebrook, A. M., Mikoviny, T., Peischl,  
892 J., Perring, A. E., Richardson, M. S., Ryerson, T. B., Schwarz, J. P., Warneke, C., Welti, A.,  
893 Wisthaler, A., Ziembka, L. D. and Murphy, D. M.: In situ vertical profiles of aerosol extinction,  
894 mass, and composition over the southeast United States during SENEX and SEAC4RS:  
895 Observations of a modest aerosol enhancement aloft, Atmos. Chem. Phys., 15(12), 7085–7102,  
896 doi:10.5194/acp-15-7085-2015, 2015.  
897 Weber, R. J., Guo, H., Russell, A. G. and Nenes, A.: High aerosol acidity despite declining  
898 atmospheric sulfate concentrations over the past 15 years, Nat. Geosci., 9,  
899 doi:10.1038/NGEO2665, 2016.  
900 Worton, D. R., Surratt, J. D., Lafranchi, B. W., Chan, A. W. H., Zhao, Y., Weber, R. J., Park, J.  
901 H., Gilman, J. B., De Gouw, J., Park, C., Schade, G., Beaver, M., Clair, J. M. S., Crounse, J.,  
902 Wennberg, P., Wolfe, G. M., Harrold, S., Thornton, J. A., Farmer, D. K., Docherty, K. S.,  
903 Cubison, M. J., Jimenez, J. L., Frossard, A. A., Russell, L. M., Kristensen, K., Glasius, M., Mao,  
904 J., Ren, X., Brune, W., Browne, E. C., Pusede, S. E., Cohen, R. C., Seinfeld, J. H. and Goldstein,  
905 A. H.: Observational insights into aerosol formation from isoprene, Environ. Sci. Technol., (47),  
906 11403–11413, doi:10.1021/es4011064, 2013.  
907 Xu, L., Suresh, S., Guo, H., Weber, R. J. and Ng, N. L.: Aerosol characterization over the  
908 southeastern United States using high-resolution aerosol mass spectrometry: Spatial and seasonal  
909 variation of aerosol composition and sources with a focus on organic nitrates, Atmos. Chem.  
910 Phys., 15(13), 7307–7336, doi:10.5194/acp-15-7307-2015, 2015a.  
911 Xu, L., Guo, H., Boyd, C. M., Klein, M., Bougiatioti, A., Cerully, K. M., Hite, J. R., Isaacman-  
912 VanWertz, G., Kreisberg, N. M., Knote, C., Olson, K., Koss, A., Goldstein, A. H., Hering, S. V.,  
913 de Gouw, J., Baumann, K., Lee, S.-H., Nenes, A., Weber, R. J. and Ng, N. L.: Effects of  
914 anthropogenic emissions on aerosol formation from isoprene and monoterpenes in the  
915 southeastern United States, Proc. Natl. Acad. Sci., 112(1), 37–42, doi:10.1073/pnas.1417609112,  
916 2015b.  
917 Xu, L., Middlebrook, A. M., Liao, J., de Gouw, J. A., Guo, H., Weber, R. J., Nenes, A., Lopez-  
918 Hilfiker, F. D., Lee, B. H., Thornton, J. A., Brock, C. A., Neuman, J. A., Nowak, J. B., Pollack,  
919 I. B., Welti, A., Graus, M., Warneke, C. and Ng, N. L.: Enhanced formation of isoprene-derived  
920 organic aerosol in sulfur-rich power plant plumes during Southeast Nexus, J. Geophys. Res.,  
921 121, 11137–11153, doi:10.1002/2016JD025156, 2016.  
922 Xu, L., Pye, H. O. T., He, J., Chen, Y., Murphy, B. N. and Ng, N. L.: Experimental and model  
923 estimates of the contributions from biogenic monoterpenes and sesquiterpenes to secondary  
924 organic aerosol in the southeastern United States, Atmos. Chem. Phys., 18(17), 12613–12637,



- 925 doi:10.5194/acp-18-12613-2018, 2018.  
926 Yu, K., Jacob, D. J., Fisher, J. A., Kim, P. S., Marais, E. A., Miller, C. C., Travis, K. R., Zhu, L.,  
927 Yantosca, R. M., Sulprizio, M. P., Cohen, R. C., Dibb, J. E., Fried, A., Mikoviny, T., Ryerson, T.  
928 B., Wennberg, P. O. and Wisthaler, A.: Sensitivity to grid resolution in the ability of a chemical  
929 transport model to simulate observed oxidant chemistry under high-isoprene conditions, *Atmos.*  
930 *Chem. Phys.*, 16(7), 4369–4378, doi:10.5194/acp-16-4369-2016, 2016.  
931 Zhang, H., Yee, L. D., Lee, B. H., Curtis, M. P., Worton, D. R., Isaacman-VanWertz, G.,  
932 Offenberg, J. H., Lewandowski, M., Kleindienst, T. E., Beaver, M. R., Holder, A. L., Lonneman,  
933 W. A., Docherty, K. S., Jaoui, M., Pye, H. O. T., Hu, W., Day, D. A., Campuzano-Jost, P.,  
934 Jimenez, J. L., Guo, H., Weber, R. J., de Gouw, J., Koss, A. R., Edgerton, E. S., Brune, W.,  
935 Mohr, C., Lopez-Hilfiker, F. D., Lutz, A., Kreisberg, N. M., Spielman, S. R., Hering, S. V.,  
936 Wilson, K. R., Thornton, J. A. and Goldstein, A. H.: Monoterpenes are the largest source of  
937 summertime organic aerosol in the southeastern United States, *Proc. Natl. Acad. Sci.*,  
938 201717513, doi:10.1073/pnas.1717513115, 2018.  
939 Zheng, Y., Unger, N., Hodzic, A., Emmons, L., Knote, C., Tilmes, S., Lamarque, J. F. and Yu,  
940 P.: Limited effect of anthropogenic nitrogen oxides on secondary organic aerosol formation,  
941 *Atmos. Chem. Phys.*, 15(23), 13487–13506, doi:10.5194/acp-15-13487-2015, 2015.  
942 Ziemann, P. J. and Atkinson, R.: Kinetics, products, and mechanisms of secondary organic  
943 aerosol formation, *Chem. Soc. Rev.*, 41(19), 6582, doi:10.1039/c2cs35122f, 2012.  
944  
945  
946

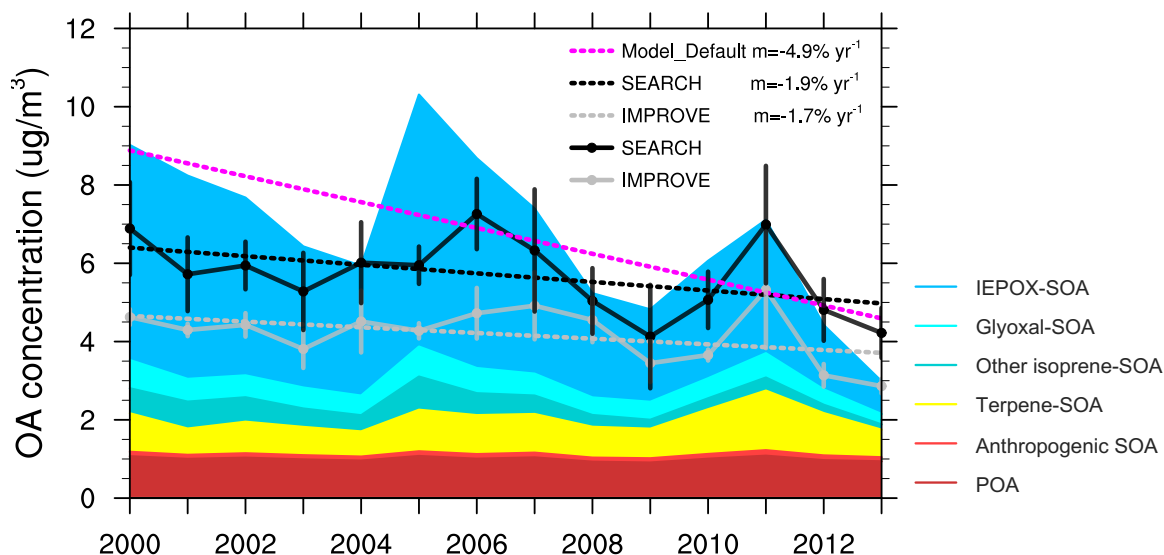


**Figure 1.** Comparison of June-July-August averaged surface OA concentration ( $\mu\text{g}/\text{m}^3$ ) over the southeast US between the default model and the observation from IMPROVE and SEARCH network. Colored shades represent different components of modeled OA. IEPOX-, glyoxal-, and other isoprene-SOA are from aqueous uptake of isoprene oxidation products. Terpene- and anthropogenic SOA are dry SOA calculated using volatility-basis-set.

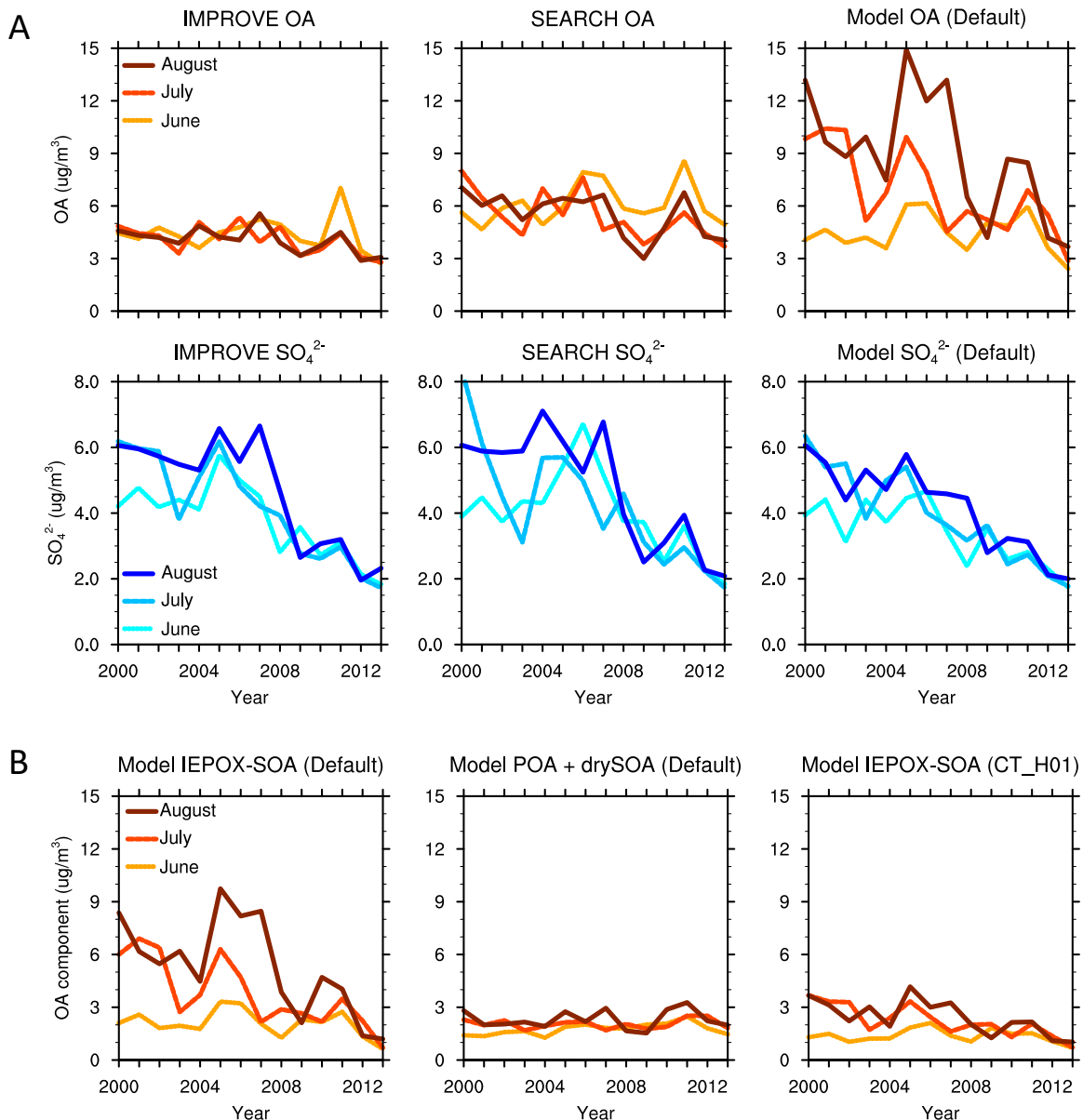


**Figure 2.** **(A)** Monthly surface OA and sulfate ( $\text{SO}_4^{2-}$ ) concentration ( $\mu\text{g}/\text{m}^3$ ) averaged over the southeast US from IMPROVE, SEARCH and the default model. **(B)** Monthly surface concentrations of IEPOX-SOA and the sum of POA and dry SOA from the default model, and IEPOX-SOA from the CT\_H01 simulation.

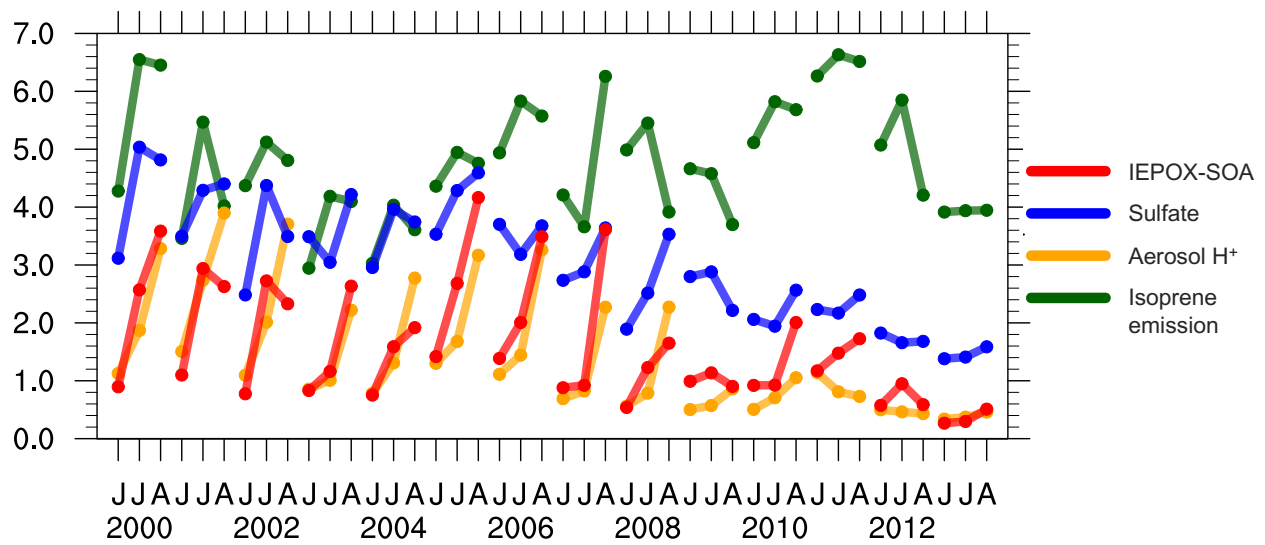


**Figure 3.** Standardized monthly surface IEPOX-SOA concentration, sulfate concentration, aerosol H<sup>+</sup> activity and isoprene emission from the default model. All variables are averaged over the southeast US, and have been divided by 1 standard deviations, therefore are unitless.

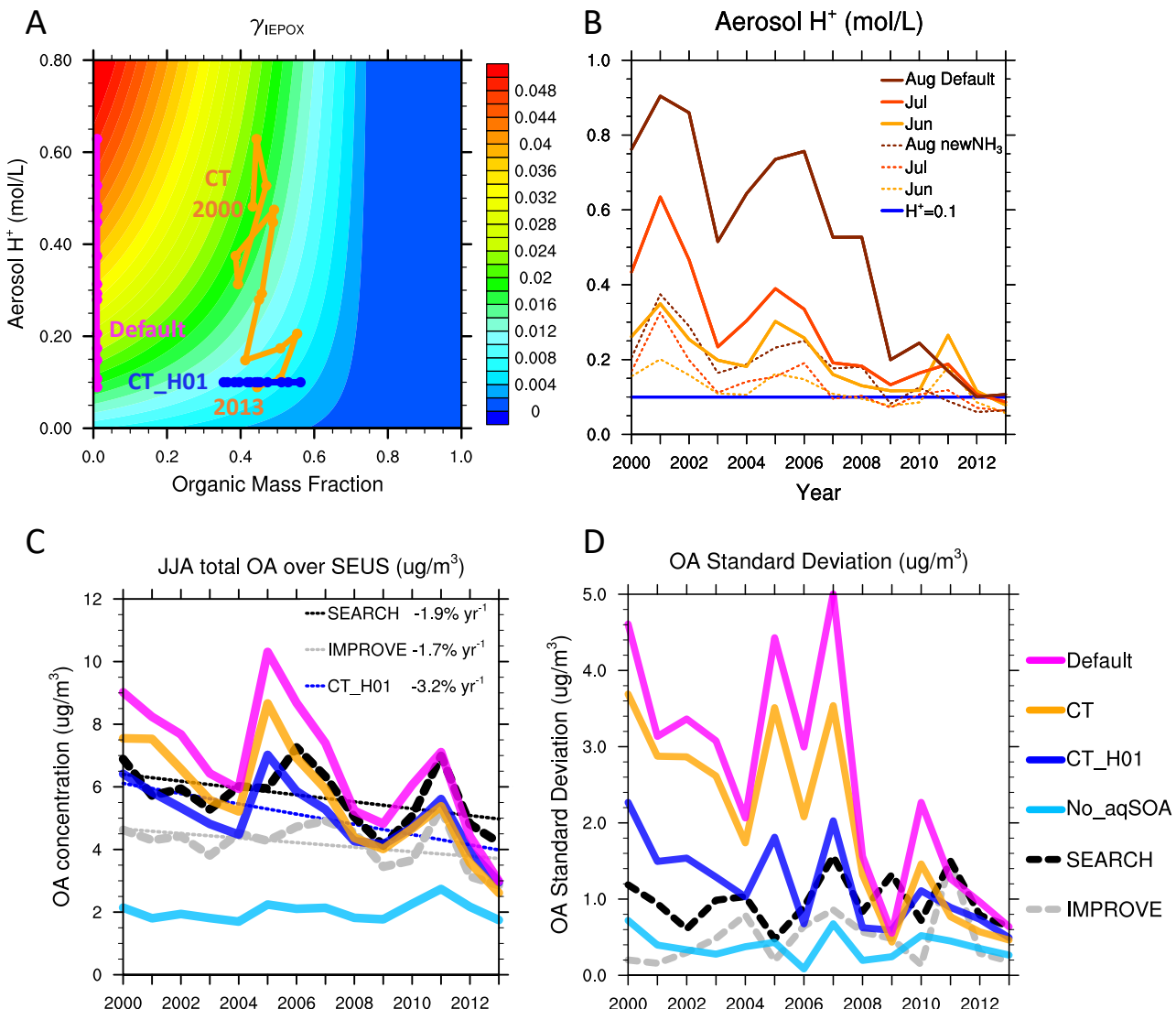


**Figure 4.** **(A)** Schematic diagram of IEPOX reactive uptake coefficient ( $\gamma_{IEPOX}$ ). Colored lines indicate the position of JJA-averaged organic mass fraction and aerosol  $H^+$  activity in 2000–2013 from the ‘Default’, ‘CT’ and ‘CT\_H01’ simulations. **(B)** Simulated aerosol acidity (mol/L) from the default, ‘CT\_newNH<sub>3</sub>’ and ‘CT\_H01’ simulations. **(C)** JJA-averaged surface OA ( $\mu\text{g}/\text{m}^3$ ) from IMPROVE, SEARCH and all model simulations. **(D)** Standard deviation of OA ( $\mu\text{g}/\text{m}^3$ ) between June, July and August from IMPROVE, SEARCH and all model simulations. All results are averaged over the southeast US.

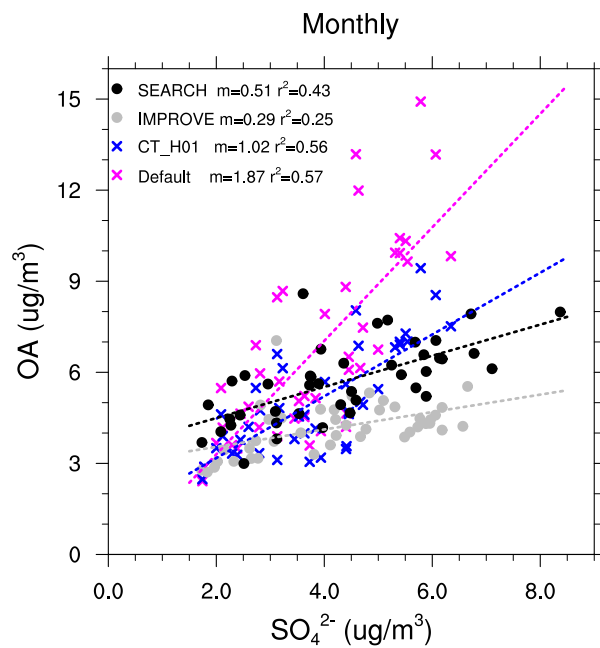


**Figure 5.** Relationships between monthly OA and sulfate concentrations ( $\mu\text{g}/\text{m}^3$ ). Each dot represents monthly data averaged from all sites from each network within the southeast US.